International Journal of Pharmaceutics 606 (2021) 120877

Contents lists available at ScienceDirect

International Journal of Pharmaceutics

journal homepage: www.elsevier.com/locate/ijpharm

Development and preclinical evaluation of microneedle-assisted resveratrol loaded nanostructured lipid carriers for localized delivery to breast cancer therapy

Shivaprasad Gadag [a], Reema Narayan [a], Archana S. Nayak [b], Diana Catalina Ardila [c], Shilpa Sant [c,d,e,f], Yogendra Nayak [g], Sanjay Garg [h], Usha Y. Nayak [a,*]

[a] Department of Pharmaceutics, Manipal College of Pharmaceutical Sciences, Manipal Academy of Higher Education, Manipal, Karnataka 576104, India
[b] Department of Chemical Engineering, National Institute of Technology Karnataka, Surathkal, Mangalore, Karnataka, 575025, India
[c] Department of Pharmaceutical Sciences, School of Pharmacy, Pittsburgh, PA 15261, USA
[d] Department of Bioengineering, Swanson School of Engineering, Pittsburgh, PA 15261, USA
[e] McGowan Institute for Regenerative Medicine, Pittsburgh, PA 15261, USA
[f] UPMC Hillman Cancer Center, Pittsburgh, PA 15261, USA
[g] Department of Pharmacology, Manipal College of Pharmaceutical Sciences, Manipal Academy of Higher Education, Manipal, Karnataka 576104, India
[h] UniSA: Clinical and Health Sciences, University of South Australia, Adelaide, SA 5000, Australia

ARTICLE INFO

Keywords:
Breast cancer
Microneedle array
Nanostructured lipid carrier
Resveratrol
Transdermal drug delivery

ABSTRACT

Resveratrol (RVT) is one of the potent anticancer phytochemicals which has shown promising potential for breast cancer therapy. However, its short half-life and low bioavailability is a major hurdle in its effective use. In this study, we have developed nanostructured lipid carriers (NLCs) of RVT to enable localized delivery of the drug to the breast tissues using microneedle arrays to improve effectiveness. The NLCs were optimized using the Design of Experiments approach and characterized for their particle size, polydispersity index, zeta potential and entrapment efficiency. The RVT-NLCs delivered using microneedle array 1200 showed a higher permeation of RVT across the skin with lower skin retention compared to pure RVT. Further, RVT-NLCs showed higher anti-cancer activity on MDA-MB-231 breast cancer cell lines and enhanced internalization compared to pure RVT. Moreover, the RVT-NLCs were found to inhibit the migration of MDA-MB-231 breast cancer cell lines. Preclinical studies in rats showed that RVT-NLCs delivered via microneedles demonstrated a remarkable increase in the C_{max}, T_{max} and $AUC_{0\text{-}inf}$, and a higher localization in breast tissue compared to pure RVT administered orally. These results suggests that the RVT-NLCs administered by microneedle array system is an effective strategy for the local delivery of RVT for breast cancer therapy.

1. Introduction

Breast cancer is the second most common cause of cancer deaths in women, impacting around 2 to 2.5 million women across the globe every year (Gadag et al., 2020; Jain et al., 2020). By 2030, breast cancer incidence is expected to rise by 50% ("Study Forecasts New Breast Cancer Cases by 2030 - National Cancer Institute," n.d.). Chemotherapy, surgery, and radiation therapies are used currently to eliminate the visible tumor. Nevertheless, chemotherapy has shown many side effects and high toxicity, thereby reducing its therapeutic potential. The main drawback of the current therapy includes toxicity to the other organs, development of resistance, which may be due to the high dose and chronic use (Shapiro and Recht, 2001). This demands safe and alternative strategies for the effective treatment of breast cancer. Recently phytoconstituents are gaining attention due to their low toxicity when compared to synthetic compounds (A. Bishayee, 2009). These phytochemicals can modulate gene expression and signaling pathways, thereby inhibiting cancer cell proliferation and overcoming resistance (Younas et al., 2018). Many researchers have reported that the phytochemicals combined with chemotherapeutic agents demonstrated reduced toxicity, synergistic effect, and increased sensitivity to multidrug-resistant breast cancer (Cragg and Pezzuto, 2016).

Resveratrol (RVT) is a naturally occurring polyphenol, which has exhibited many biological activities namely anti-tumor, anti-

* Corresponding author.
E-mail address: usha.nayak@manipal.edu (U.Y. Nayak).

https://doi.org/10.1016/j.ijpharm.2021.120877
Received 9 March 2021; Received in revised form 8 June 2021; Accepted 7 July 2021
Available online 10 July 2021

inflammatory, anti-viral, anti-oxidant, cardioprotective, neuroprotective, and antiaging (Carter et al., 2014; Chedea et al., 2017; Cho et al., 2017; Ko et al., 2017; Kotecha et al., 2016; Nawaz et al., 2017; Xiao et al., 2019). RVT affects all three stages of carcinogenesis such as tumor initiation, promotion, and progression, by altering the pathways that control cell growth, cell division, angiogenesis, inflammation, apoptosis, and metastasis (Anupam Bishayee, 2009). Many researchers have accorded RVT as a promising therapy for cancer prevention and chemotherapeutic effects on breast cancer (Ko et al., 2017; Sinha et al., 2016a). Hao and co-workers formulated folic acid-decorated micelles to enhance the water solubility and target the tumor cell to effectively treat breast cancer and have proved its efficacy on MCF-7 breast cancer cell lines (Hao et al., 2017). Despite the proven benefits of RVT in breast cancer treatment, its use is restricted due to very low oral bioavailability owing to its extensive first-pass metabolism and rapid elimination (Sinha et al., 2016b). Moreover, RVT has other drawbacks such as low aqueous solubility (<0.05 g/L), photolytic instability, and low permeability across the stratum corneum (Robinson et al., 2015; Silva et al., 2013; Tosato et al., 2018). To overcome these limitations RVT is encapsulated into the nanocarriers. Poonia and coworkers successfully incorporated RVT into the nanostructured lipid carriers (NLCs) decorated with folic acid for intravenous administration. The cytotoxicity studies showed a lower IC_{50} of the RVT loaded NLCs with and without folic acid decoration when compared to pure RVT in MCF-7 cell lines. The preclinical studies showed an increase in AUC of RVT loaded NLCs when compared with pure RVT, in the rats (Poonia et al., 2019).

The transdermal route of administration is another viable alternative, which can bypass the first-pass metabolism, thereby increasing the bioavailability of RVT and also provide a localized delivery of the drug. Tosato and co-workers have developed various liposomal formulations for the transdermal delivery of RVT (Tosato et al., 2018). Literature is available wherein RVT has been incorporated into the NLCs, and used for the testing of its antioxidant (Gokce et al., 2012), and antiaging potential on dermal application (Hidayah et al., 2018). The use of a microneedle (MN) delivery system helps in breaching the skin's barrier and facilitates the delivery of the drug locally or systemically. Bhatnager and team, developed zein MN loaded with gemcitabine and tamoxifen for localized therapy for breast cancer treatment (Bhatnagar et al., 2018). Similarly, dissolvable MN patches with docetaxel and doxorubicin have been fabricated for the treatment of breast cancer (Bhatnagar et al., 2019). In one of our previous studies, we have successfully used an MN array system to deliver pH-sensitive Solulan tailored niosomes loaded with donepezil for brain targeted delivery (Nayak et al., 2020).

Based on this background, in the present study, we have developed NLCs loaded with RVT coupled with MN array assisted delivery system for the local delivery of RVT to improve the therapeutic concentration at the site of action. The *in vitro* efficacy of the developed RVT loaded NLCs were studied in MDA-MB-231 breast cancer cell lines, and preclinical studies were performed in Sprague-Dawley rats. To the best of our knowledge, this is the first comprehensive characterization of a MN-assisted delivery system of RVT loaded NLCs for the localized treatment of breast cancer.

2. Materials and methods

2.1. Materials

RVT (>99.0%), glyceryl monostearate (GMS), cetyl palmitate (CP), glyceryl di-stearate (GDS), glyceryl monooleate (GMO) were procured from TCI Chemicals Pvt. Ltd., India. Oleic acid (OA), trifluoroacetic acid (TFA), poloxamer 188 (P188), stearic acid (SA), tween 80 (T80), tween 20 (T20), carbopol 934, triethanolamine, acetonitrile (ACN, HPLC grade), methanol (HPLC grade) were purchased from Merck Ltd., India. Labrafac PG (LP), labrasol (LB), labrafil (LF), miglyol 810 (MG) and capryol 90 (C90), compritol ATO888 (CA) were a generous gift from Gattefosse India Pvt. Ltd., India. Fluorescein isothiocyanate (FITC) and resazurin were procured from Sigma-Aldrich Co., USA.

2.2. Screening of excipients

The lipids (solid and liquid) and surfactants were selected based on their ability to solubilize RVT. The solubility of RVT in solid lipids (GMS, SA, CP, CA, and GDS) was tested by heating the lipids 5 °C above their melting point, and gradual addition of RVT into the molten lipid until undissolved RVT was observed. The solubility of RVT in liquid lipids (OA, GMO, LP, MG, and C90) and surfactant T20, T80, P188, LF, and LB, 1% w/v aqueous solution was performed by adding an excess amount of RVT keeping them in a shaking water bath for 48 h. The samples were centrifuged at 16000*xg* for 30 min, followed by analyzing the supernatant using reverse-phase high-performance liquid chromatography (RP-HPLC) (Singh and Pai, 2014).

2.3. Preparation of NLCs

NLCs were prepared by melt-emulsification method followed by size reduction using a probe sonicator (VibraCell™, VC 130, Sonics and Materials Inc., USA) as previously reported (Managuli et al., 2019). GMS and C90 mixture were heated to 80 °C, to this accurately weighed RVT was added and solubilized. To this, preheated (80 °C) surfactant solution was added under stirring. The so-formed primary emulsion was probe-sonicated to obtain NLCs. Similarly, the FITC loaded NLCs were prepared by incorporating FITC-conjugated stearylamine as per the previously reported method (Patel et al., 2018; Yuan et al., 2008, 2007).

2.4. Statistical optimization of NLCs

The screening of the variables and the formulation optimization was performed using the Design of Experiments approach using Minitab® 18. For the screening of independent variables, the Plackett-Burman design was adopted. The variables considered for the preparation of NLCs along with their limits are presented in Table 1. Following the screening, the optimization of the independent variables was carried out using response surface methodology, Box-Behnken design (Jazuli et al., 2019). It involves a bunch of mathematical and statistical methods used for modeling and analyzing the experimental framework. The factors with $p < 0.05$ were considered to be influencing the responses significantly. Attributes that were considered for building Box-Behnken design are presented in Table 2. Response surface plots are used to understand the interaction between two variables by keeping the third variable constant, as a function of the 3D graph, where variables are plotted on

Table 1
Variables considered in Plackett-Burman design.

Factors	Lower limit (−1)	Higher limit (+1)
Material attributes		
X1: Total lipid (mg)	70	150
X2: Surfactant concentration (%)	0.5	3
X3: Oil (%) (with respect to total lipid)	5	30
X4: Drug (%) (with respect to total lipid)	5	15
Process parameters		
X5: Sonication amplitude (%)	20	40
X6: Sonication pulse (sec)	5	10
X7: Sonication time (min)	1	5
X8: Temperature (°C)	70	90

Table 2
Variables considered for optimization using Box-Behnken design.

Factors	Lower limit (−1)	Higher limit (+1)
Y1: Total lipid (mg)	90	130
Y2: Surfactant concentration (%)	1	2
Y3: Oil (%) (with respect to total lipid)	5	15
Y4: Drug (%) (with respect to total lipid)	5	15

X, Y-axes, and response on Z-axes (Kumar and Sawant, 2013; "Overview for Surface Plot - Minitab," n.d.).

2.4.1. Robustness of the generated design space

The design space was obtained by overlaying the contour plots using Minitab® 18 by entering the desired value of responses. Validation of the established design space in the Box-Behnken design is a pivotal factor required from the scale-up point of view. It is essential to investigate and assess whether the practical design space yields the desired response and if the undesired responses are obtained outside the design space to assess its robustness. For assessing the robustness of the design space three points were considered; at the center, on the border, and outside the generated design space. The error was calculated between the software suggested values and the obtained experimental results.

2.5. Characterization of NLCs

The particle size (PS), polydispersity index (PDI), and zeta potential (ZP) of the NLCs were measured using Malvern Zetasizer (Nano ZS, Malvern Instruments; Malvern, UK) with the appropriate dilution of samples. The optimized formulation was subjected to centrifugation at 18000*xg* for 1.5 h, and the collected pellet was re-dispersed in water and lyophilized. The lyophilized formulations were analyzed using FT-IR 8300 spectrophotometer (Shimadzu, Tokyo, Japan). The samples were prepared by the pressed pellet method using potassium bromide and scanned from 4000 to 400 cm^{-1}. DSC thermograms were recorded using a DSC-60 calorimeter (Shimadzu, Kyoto, Japan) by heating from 25 °C to 300 °C, at a rate of 10 °C per minute under nitrogen flow (50 mL/min). The solid-state characterization of the samples was performed by studying the X-ray diffraction pattern (Philips, PW-171 x-ray diffractometer) for assessing any change in the crystal nature of the drug during entrapment. The surface morphology and size of the NLCs were studied by high resolution- transmission electron microscopy (HR-TEM) analysis (Jeol/JEM 2100, LaB6).

2.6. Entrapment efficiency (EE)

EE of the formulated NLCs was determined by gel chromatographic technique, using Sephadex G-50 column (2 cm length × 1 cm diameter) (CH et al., 2014; Gu et al., 2011; Managuli et al., 2019; Zhang et al., 2014). Briefly, Sephadex G-50 was allowed to swell by soaking in water for 12 h at room temperature after which the gel was packed into a syringe and centrifuged at 1500*xg* for about 2 min. Later, the column was hydrated by adding 0.5 mL of water, following which 0.5 mL of NLCs suspension was passed through the column. 0.5 mL of water was further added for the complete elution of NLCs. The collected turbid suspension was treated with methanol to rupture the NLCs, centrifuged at 16000*xg* for 10 min, and the supernatant was analyzed using RP-HPLC with suitable dilutions (Singh and Pai, 2014).

2.7. Preparation and evaluation of NLCs incorporated into carbopol

The optimized NLCs formulation was incorporated into carbopol (0.1% w/v) as a thickening agent, which was neutralized with triethanolamine (Al-malah, 2014; Lubrizol, 2010). Benzoic acid (0.1% w/v) was added as a preservative and ascorbic acid (0.3%) as an antioxidant. The viscosity of the formulation was determined using Brookfield programmable rheometer (Brookfield, LVDV-III U CP, USA). The formulation is denoted as RVT-NLCs-CP in this manuscript. Drug content of the formulation was determined by treating the formulation with methanol followed by estimating the amount of drug present using RP-HPLC with suitable dilution.

2.8. In vitro drug release study

The RVT release from RVT-NLCs and RVT-NLCs-CP was examined using the dialysis bag method (Bohrey et al., 2016). 2 mL of the formulation was transferred into a preactivated dialysis bag (12 kDa cut-off) and sealed on both ends. This was placed in 200 mL of phosphate buffer saline (PBS), pH 7.4, maintained at 37 ± 2 °C for 48 h. The samples were collected at predetermined time intervals and analyzed using RP-HPLC with appropriate dilutions.

2.9. Skin permeation and retention study using hollow microneedles

The permeation study was performed using porcine ear skin obtained from a local slaughterhouse. The porcine skin was then sandwiched between the donor and receptor compartment of the Franz diffusion cell (Orchid Scientific, India), the dermis facing towards the donor compartment. The receptor compartment was filled with pH 7.4 PBS maintained at 32 ± 2 °C and 450 rpm. For the experiment, three different dimensions of the microneedle array system were used namely 600, 777, and 1200 (AdminPatch® Microneedle Arrays, Nano-BioScience LLC, CA, USA) denoted as 600 MN, 777 MN, and 1200 MN in this manuscript. The hollow microneedle arrays were gently pressed on the porcine skin. The skin with the microneedle array system was kept undisturbed throughout the experiment (Nayak et al., 2020). After setting up the skin (Fig. 1) with microneedle arrays in the Franz diffusion cell, the donor compartment was filled with 2 mL of RVT-NLCs-CP, and the experiment was carried out for 24 h. The samples were collected at predetermined time intervals, treated with methanol (to rupture the intact NLCs), and analyzed using RP-HPLC after suitable dilution. At the end of the experiment, the skin was homogenized in PBS, extracted with methyl t-butyl ether (MTBE), and the samples were analyzed using RP-HPLC.

2.10. Accelerated stability studies

The stability studies of the optimized formulation (RVT-NLCs-CP) was performed as per the International Council for Harmonization of Technical Requirements for Pharmaceuticals for Human Use (ICH) Q1A (R2) guidelines at 5 ± 3 °C and 25 ± 2 °C/60 ± 5% RH for four months. The stability of the formulation was assessed by the change in the viscosity, drug content, and drug release (International Conference on Harmonisation Guidelines, 2003; Nagaich and Gulati, 2016).

2.11. In vitro cell line studies

2.11.1. Cytotoxicity assay

Cytotoxicity studies of the optimized NLCs were carried out on MDA-MB-231 breast cancer cell lines using alamarBlue assay (Bonnier et al., 2015; Tahara et al., 2017). Cells were seeded in 96-well plates in 180 μL of Dulbecco's Modified Eagle Medium (DMEM) containing 10% heat-inactivated fetal bovine serum (FBS), and 1% v/v antibiotics (penicillin and streptomycin) at a density of 1×10^4 cells per well. The cells were allowed to adhere in the incubator at 37 °C, 5% CO_2. After 24 h of incubation, the cells were treated with 20 μL of RVT solution in 0.8% DMSO, or RVT loaded NLCs in PBS or placebo NLCs in PBS. The final concentration of RVT in each well ranged from 0.1 μg/mL-100 μg/mL. After 48 h of treatment, media from each well was replaced with 200 μL of resazurin solution (10% w/v) in media and incubated for another 3 h (Uzunoglu et al., 2010). Fluorescence intensity was measured at 530/590 nm using a plate reader (SpectraMax m5e, Molecular Devices, USA).

2.11.2. Cellular uptake study

Cellular uptake of RVT loaded NLCs was performed on MDA-MB-231 breast cancer cell lines. Cells were seeded in sterile 24-well plates at a concentration of 1.2×10^5 cells per well and incubated for 24 h to allow cell adhesion. The cells were treated with FITC loaded NLCs. After predetermined time intervals (1 h, 2 h, 4 h, and 6 h), the cells were washed 3 times with PBS to remove the free NLCs that were not uptaken by the cells. The cells were then fixed with 4% paraformaldehyde, and

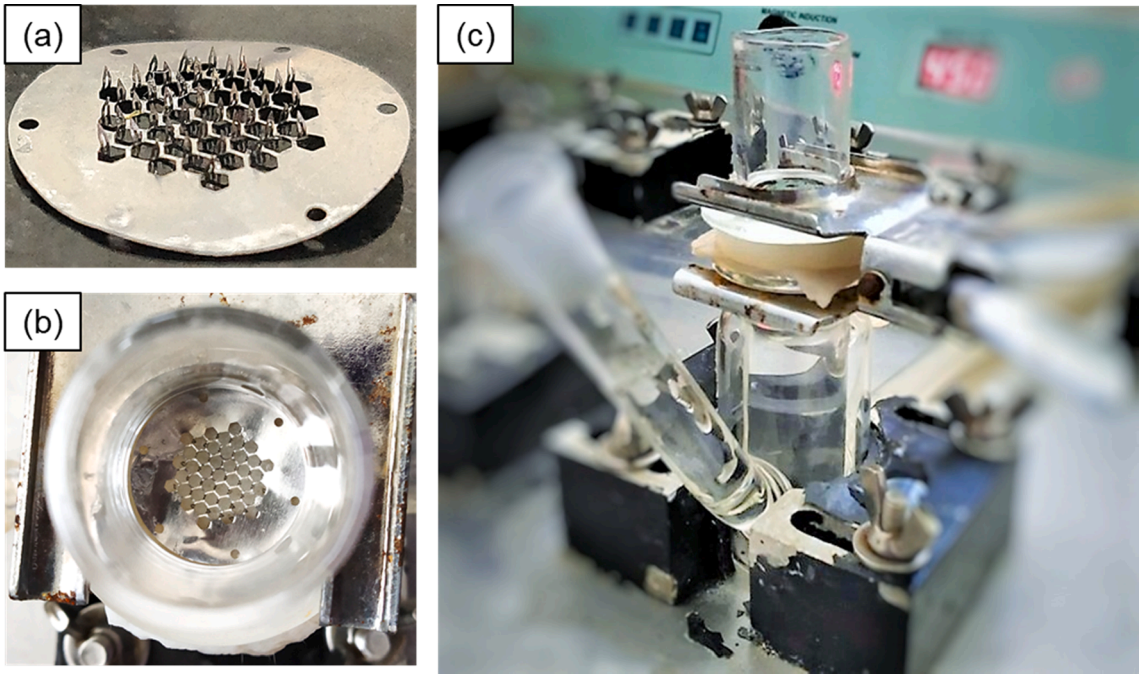

Fig. 1. Photographs of (a) Microneedle array (1200 MN), skin with microneedle array system in Franz diffusion cell (b) top view, and (c) side view.

nuclei were stained with Hoechst solution (Farooq et al., 2019; Kayani et al., 2018). The cellular uptake profile was determined by recording integrated fluorescence density per cell using a confocal laser microscope (FV1000 SPD, Olympus, USA). Fluorescence intensity per cell was measured using Fiji – ImageJ software (*Basic Intensity Quantification with ImageJ*, n.d., "Measuring cell fluorescence using ImageJ — The Open Lab Book v1.0," n.d.; Miura, 2020).

2.11.3. Cell migration assay

The cell migration assay was performed using MDA-MB-231 cells seeded in a 96-well plate at a density of 5×10^5 cells per well. After 24 h, a scratch to the monolayer was made using a 200 μL pipette tip, followed by washing with PBS three times to remove the detached cells. The scratched cell monolayer was treated with the IC_{50} concentration of RVT solution and RVT-loaded NLCs, (n = 3). The plates were then incubated in a CO_2 incubator and imaged at 0, 12, and 24 h using a light microscope (Carl Zeiss Microscopy, Germany). The wound width (the scratch segment that remained open) was measured using Fiji – ImageJ software (10 measurements were taken for each image). To compare the groups, a two-way ANOVA with a Post-Hoc analysis using Tukey's test was performed using GraphPad Prism® 8.0 (La Jolla, CA, USA).

2.12. Preclinical pharmacokinetic and tissue distribution studies

2.12.1. Animals

Female Sprague Dawley rats weighing between 180 and 200 g were obtained from the Central Animal Research Facility, Manipal Academy of Higher Education, Manipal. The rats were housed in polypropylene cages with access to food and water *ad libitum*, acclimatized to 12 h light/dark cycles at a temperature of 25 ± 3 °C and relative humidity 65 ± 5%. The studies were performed as per the guidelines framed by the Committee for Control and Supervision of Experiments on Animals (CPCSEA) and the approved protocol (IAEC/KMC/33/2017).

2.12.2. Experimental design for pharmacokinetic studies

The Sprague Dawley rats were randomly divided into three groups of six each. They were treated as per the following design:

Group 1: RVT *p.o.* at a dose of 20 mg/kg
Group 2: RVT-NLCs-CP subcutaneous (SC) at a dose of 20 mg/kg (equivalent to RVT)
Group 3: RVT-NLCs-CP via MN array at a dose of 20 mg/kg (equivalent to RVT)

Blood was withdrawn periodically and collected in a tube containing 10% EDTA. The plasma was collected by centrifugation and stored at −80 °C till the estimation of RVT in it. The amount of RVT in the plasma was quantified as per the previously reported RP-HPLC method (Chen et al., 2007). The pharmacokinetic parameters, namely C_{max}, T_{max}, area under the curve (AUC), mean residence time (MRT), and elimination rate (Ke) was determined using PK Solutions 2.0™. The student's *t*-test was used to analyze the difference between the group 3 vs group 1, and group 3 vs group 2 using GraphPad Prism® 8.0 (La Jolla, CA, USA).

2.12.3. Tissue distribution studies

To quantify the amount of RVT in the breast tissue, rats were divided into two groups consisting of twenty one rats in each group and treated as per those in group 1 and group 3 in pharmacokinetic studies (Section 2.12.2). At predetermined time intervals, rats were sacrificed, and breast tissue was collected. The collected tissues were homogenized and RVT present in the tissue was quantified using RP-HPLC. The student's *t*-test was used to analyze the difference between the groups using GraphPad Prism® 8.0 (La Jolla, CA, USA).

3. Results and discussion

The present work involves the design, development, and evaluation of RVT loaded NLCs wherein the variables affecting the particle size,

PDI, zeta potential, and entrapment efficiency of NLCs were screened and optimized. The working range of the variables was finalized followed by its optimization using the Design of experiments. The *ex vivo* permeation studies of the optimized NLCs were performed using MN arrays. Further *in vitro* efficacy testing was performed in MDA-MB-231 breast cancer cell lines.

3.1. Solubility studies

RVT showed maximum solubility in GMS among the chosen solid lipids. This may be due to the hydrogen bonding between the hydroxy group of RVT and GMS, and the lipophilic interactions between the stearyl chain of GMS and benzene rings of RVT. Similarly, RVT exhibited the highest solubility in capryol 90 (liquid lipid) and least solubility in 1% w/v of poloxamer 188 surfactant solution. Therefore, GMS, capryol 90, and poloxamer 188 were selected as the solid lipid, liquid lipid, and surfactant, respectively for the development of NLCs. The solubility of RVT in different lipids and surfactants is shown in Fig. 2. An appropriate blend of solid lipid and liquid lipid helps in the improvement of entrapment efficiency by reducing the crystallinity of RVT and preventing the expulsion of the drug during storage (Haider et al., 2020; Subramaniam et al., 2020).

3.2. Optimization of the NLCs using a statistical model

3.2.1. Screening of the independent variables

The screening of independent variables (total lipid, surfactant concentration (%), oil (%), drug (%), sonication amplitude, sonication pulse, sonication time, temperature) was performed using the Plackett-Burman design. Plackett-Burman design is useful in the preliminary screening studies to identify the main factors influencing the responses from a large number of factors (Vatanara et al., 2007).

Pareto charts were used to determine significant factors among independent variables. One-way ANOVA was performed for the same, and factors with $p < 0.05$ were considered to be statistically significant. The experimental responses observed in the Plackett-Burman design are depicted in Table 3.

The Pareto chart (Fig. 3) gives the visual impression of the significant factors influencing the desired responses. It was observed that the surfactant concentration, total lipid, oil (%), and drug (%) showed a significant influence on the dependent variables. Surfactant concentration was the topmost factor followed by total lipid, which was significantly influencing particle size. Similarly, total lipid was the highest influencing factor on the entrapment efficiency followed by surfactant concentration, oil (%), and drug (%). However, the independent variables did not significantly influence the PDI and zeta potential of the NLCs at

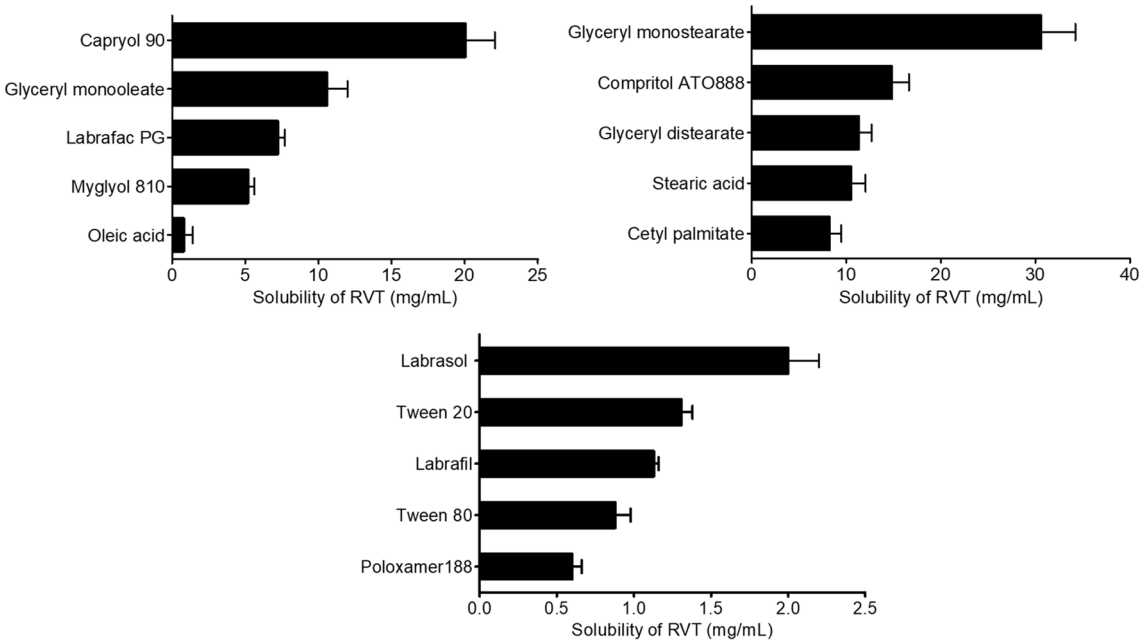

Fig. 2. Solubility of RVT in (a) Solid lipids, (b) Liquid lipids and (c) Surfactant solutions (1% w/v).

Table 3
Summary of results obtained for Plackett-Burman design.

Batches	X1	X2	X3	X4	X5	X6	X7	X8	Particle size (nm)	PDI	Zeta potential (mV)	%EE
PB-1	70	0.5	5	15	40	10	1	90	200.45 ± 10.12	0.383 ± 0.055	−6.32 ± 0.35	59.23 ± 1.4
PB-2	150	3	5	15	20	5	1	90	134.20 ± 5.87	0.302 ± 0.048	−8.86 ± 0.53	60.06 ± 4.67
PB-3	70	3	30	5	40	5	1	70	99.25 ± 4.35	0.440 ± 0.086	−8.60 ± 0.35	34.45 ± 1.98
PB-4	150	3	30	5	40	10	1	90	120.23 ± 5.63	0.278 ± 0.073	−4.06 ± 0.22	66.02 ± 5.27
PB-5	70	3	30	15	20	10	5	70	97.39 ± 7.92	0.366 ± 0.059	−10.60 ± 0.81	48.39 ± 2.44
PB-6	70	0.5	30	15	40	5	5	90	180.51 ± 12.48	0.448 ± 0.093	−9.20 ± 0.37	46.81 ± 3.09
PB-7	150	0.5	5	5	40	10	5	70	350.01 ± 9.54	0.280 ± 0.074	−10.30 ± 0.76	88.73 ± 5.68
PB-8	150	0.5	30	5	20	5	5	90	356.70 ± 11.2	0.388 ± 0.061	−10.50 ± 0.68	79.10 ± 3.79
PB-9	150	0.5	30	15	20	10	1	70	384.50 ± 10.73	0.655 ± 0.079	−12.50 ± 0.94	70.07 ± 3.67
PB-10	70	3	5	5	20	10	5	90	95.46 ± 4.71	0.403 ± 0.053	−9.01 ± 0.69	62.39 ± 2.21
PB-11	150	3	5	15	40	5	5	70	120.04 ± 6.88	0.435 ± 0.071	−8.86 ± 0.48	61.11 ± 2.65
PB-12	70	0.5	5	5	20	5	1	70	156.31 ± 8.29	0.380 ± 0.065	−10.50 ± 0.94	69.24 ± 3.16

X1 = Total lipid (mg), X2 = Surfactant concentration (%), X3 = Oil (%), X4 = Drug (%), X5 = Sonication amplitude (%), X6 = Sonication pulse (sec), X7 = Sonication time (min), X8 = Temperature (°C).

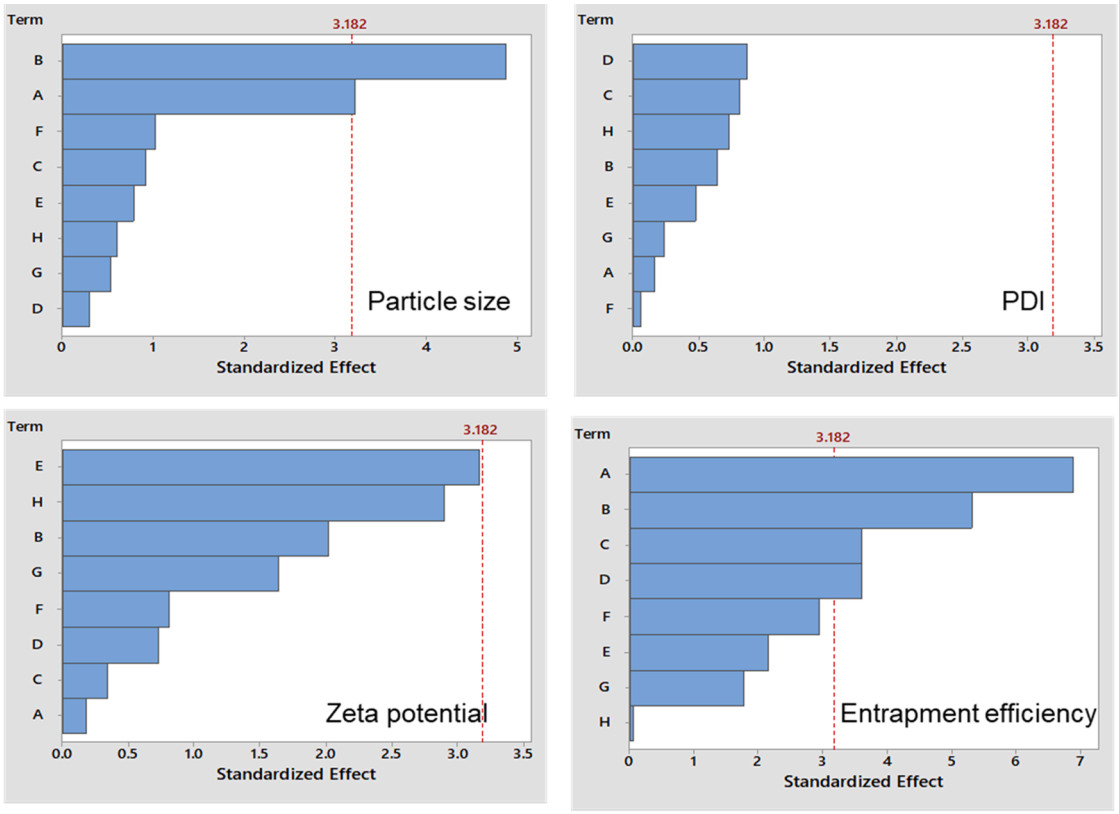

Fig. 3. Pareto chart showing the effect of independent variables from Plackett-Burman design.

the levels studied. Out of the eight independent variables, only the material attributes significantly influenced the dependent variables. As the process parameters did not affect the outcome, we carried out further optimization of NLCs by maintaining the sonication time, amplitude, and pulse at 5 min, 40%, and 10 sec respectively, with a temperature of 80 °C.

3.2.2. *Statistical optimization of the independent variables*

Based on the results of preliminary screening using Plackett-Burman design, the effect of the material attributes, total lipid, surfactant concentration, oil (%), and drug (%) were further investigated on the desired responses of NLCs using Box-Behnken design. The Box-Behnken design was used to optimize and evaluate the main effects, interaction effects, and quadratic effects of the process variables. A total of 27 runs along with the responses obtained are summarized in Table 4. The influence of the independent variables on the outcome was assessed from the three-dimensional surface plot. The positive sign of the coefficients indicates a positive influence on the variables, whereas the negative sign reveals a negative effect. The Pareto chart showing the main effects, interaction effects, and effects of squared factors on the particle size, PDI, zeta potential, and entrapment efficiency is shown in Fig. 4.

3.2.2.1. Effect of independent variables on particle size. The particle size of NLCs was found to be in the range of 103.48 ± 3.65 nm to 708.3 ± 12.84 nm. We observed that the higher the surfactant concentration, the smaller the particle size. This could be explained by the theory that higher surfactant concentration stabilizes the formed nanoparticle by completely covering their surface and thereby preventing the coalescence of smaller particles into bigger particles (Kaur et al., 2016; Zirak and Pezeshki, 2015). The total lipid concentration showed a positive influence on the particle size. The increase in the particle size with an increase in the lipid could be attributed to increased lipid phase viscosity, thus reducing the shearing capacity of the probe sonicator (Emami et al., 2015). Amongst all the independent variables, the surfactant concentration exhibited the maximum influence on the particle size observed from its F-value. The regression equation for particle size, presenting the significant factors is shown in Eq. (1).

$$\begin{aligned} Particle\ size\ =\ &-177\ +\ 6.8\ [Total\ lipid]\ -\ 342\ [Surfactant] \\ &+\ 583.1\ [Surfactant^{*}\ Surfactant] \\ &-\ 13.12\ [Total\ lipid^{*}\ Surfactant] \end{aligned} \tag{1}$$

3.2.2.2. Effect of independent variables on PDI. The PDI of the formulation batches was found to range between 0.201 ± 0.027 and 0.502 ± 0.062. As the surfactant concentration increased, the PDI was found to decrease, which was evident from the results. This may be due to the reduction in the surface tension between the lipid and aqueous phase with an increase in the surfactant concentration, thereby providing a better mixing and uniform distribution of shear during sonication (Koh et al., 2014). The total lipid concentration showed a positive effect on the PDI. This can be explained by the increase in the viscosity of the lipid phase with an increase in the lipid concentration which restricts the uniform distribution of shear during sonication, thus leading to the heterogeneous distribution of particles. Among all the independent variables under study, the surfactant concentration showed a maximum influence on the PDI of the NLCs. The regression equation for PDI

Table 4
Summary of the results obtained using Box-Behnken design.

Batches	Y1	Y2	Y3	Y4	Particle size (nm)	PDI	Zeta potential (mV)	%EE
BB-1	90	1.5	5	10	110.48 ± 4.72	0.224 ± 0.031	−6.32 ± 0.46	62.43 ± 2.63
BB-2	110	1.5	15	5	109.61 ± 3.76	0.262 ± 0.028	−10.86 ± 0.51	81.91 ± 3.41
BB-3	90	1.5	10	15	143.48 ± 6.02	0.339 ± 0.035	−8.61 ± 0.47	58.03 ± 2.62
BB-4	130	1.5	10	5	195.50 ± 6.83	0.336 ± 0.027	−4.06 ± 0.24	87.45 ± 2.48
BB-5	110	1.5	10	10	110.03 ± 3.09	0.218 ± 0.031	−6.60 ± 0.33	79.92 ± 4.01
BB-6	110	1.0	10	15	526.14 ± 4.46	0.651 ± 0.048	−9.20 ± 0.58	79.34 ± 3.85
BB-7	110	2.0	10	15	108.52 ± 3.68	0.215 ± 0.032	−7.83 ± 0.46	57.43 ± 3.36
BB-8	130	2.0	10	10	123.53 ± 4.32	0.209 ± 0.019	−8.52 ± 0.32	72.31 ± 2.34
BB-9	110	2.0	15	10	110.01 ± 2.59	0.211 ± 0.039	−11.50 ± 0.52	68.06 ± 3.75
BB-10	110	1.5	15	15	134.28 ± 2.48	0.286 ± 0.045	−10.50 ± 0.48	68.74 ± 2.56
BB-11	110	2.0	10	5	106.32 ± 3.65	0.213 ± 0.036	−8.86 ± 0.59	78.91 ± 3.33
BB-12	130	1.5	10	15	202.46 ± 4.24	0.325 ± 0.028	−7.51 ± 0.42	82.64 ± 4.21
BB-13	110	1.5	10	10	110.02 ± 2.76	0.218 ± 0.034	−6.62 ± 0.33	79.92 ± 3.76
BB-14	130	1.5	5	10	188.92 ± 4.93	0.358 ± 0.038	−4.46 ± 0.27	83.21 ± 2.64
BB-15	110	2.0	5	10	107.89 ± 3.52	0.208 ± 0.040	−5.01 ± 0.38	67.58 ± 3.32
BB-16	110	1.5	5	5	109.15 ± 4.26	0.216 ± 0.046	−5.06 ± 0.42	83.02 ± 4.27
BB-17	110	1.0	15	10	492.47 ± 10.43	0.489 ± 0.076	−10.65 ± 0.73	84.51 ± 4.35
BB-18	110	1.5	10	10	110.06 ± 4.02	0.218 ± 0.034	−6.61 ± 0.47	79.92 ± 4.84
BB-19	110	1.5	5	15	108.66 ± 3.54	0.203 ± 0.035	−4.33 ± 0.36	69.63 ± 2.66
BB-20	90	1.0	10	10	163.67 ± 5.38	0.307 ± 0.064	−6.50 ± 0.35	76.52 ± 3.46
BB-21	90	1.5	10	5	107.51 ± 2.76	0.245 ± 0.028	−8.50 ± 0.49	73.68 ± 2.57
BB-22	130	1.5	15	10	198.84 ± 4.46	0.263 ± 0.053	−9.98 ± 0.62	83.34 ± 3.39
BB-23	110	1.0	10	5	315.60 ± 7.36	0.385 ± 0.032	−7.84 ± 0.59	84.55 ± 4.68
BB-24	130	1.0	10	10	708.32 ± 12.84	0.668 ± 0.047	−8.50 ± 0.61	86.20 ± 2.95
BB-25	110	1.0	5	10	408.68 ± 6.34	0.502 ± 0.062	−4.32 ± 0.36	85.57 ± 3.43
BB-26	90	2.0	10	10	103.48 ± 3.65	0.201 ± 0.027	−8.86 ± 0.53	48.23 ± 5.32
BB-27	90	1.5	15	10	109.52 ± 3.98	0.223 ± 0.023	−9.60 ± 0.72	58.91 ± 2.02

Y1 = Total lipid (mg), Y2 = Surfactant concentration (%), Y3 = Oil (%), Y4 = Drug (%),

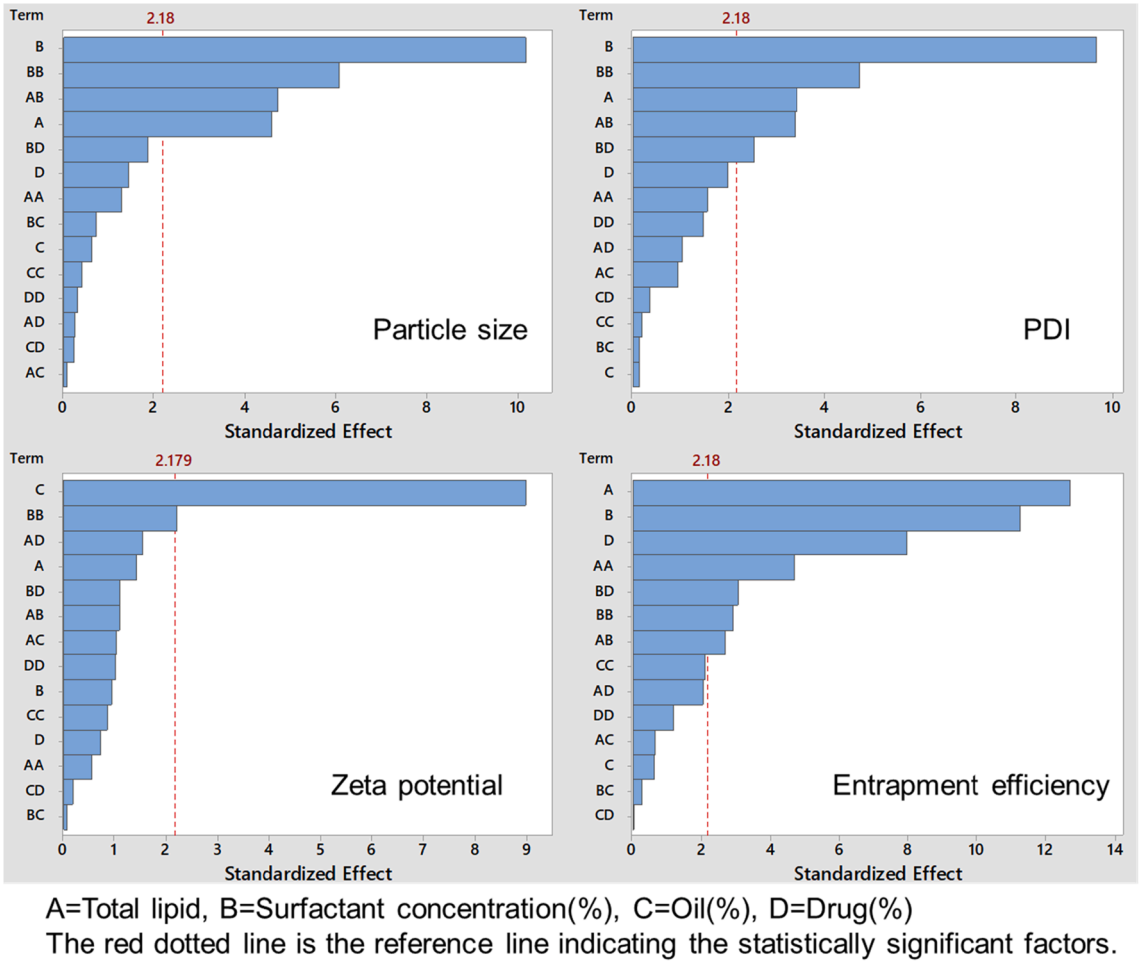

Fig. 4. Pareto chart showing the effect of independent variables from Box-Behnken design.

presenting the significant factors is shown in Eq. (2).

$$PDI = 0.13 + 0.0016\,[Total\ lipid] - 0.352\,[Surfactant] + 0.4265\,[Surfactant*Surfactant] - 0.00882\,[Total\ lipid*Surfactant] - 0.0264\,[Surfactant\ conc*Drug] \quad (2)$$

3.2.2.3. Effect of independent variables on zeta potential. The zeta potential varied between −4.06 ± 0.24 mV and −11.5 ± 0.52 mV. The oil content showed a positive effect on the zeta potential. Enhanced repulsion between the NLCs is expected with a higher zeta potential. The surfactant used in the study, poloxamer 188, is a high molecular weight, non-ionic surfactant which will sterically stabilize the NLCs despite the low zeta potential (Han et al., 2008). The regression equation for zeta potential presenting the significant factors is shown in Eq. (3).

$$Zeta\ potential = -25.6 + 0.445\,[Oil] - 4.13\,[Surfactant*Surfactant] \quad (3)$$

3.2.2.4. Effect of independent variables on entrapment efficiency (EE). The entrapment efficiency of the various batches of NLCs ranged from 48.23 ± 5.32% to 87.45 ± 2.48%. It was observed that the higher the total lipid concentration, the greater is the % EE, which may be due to the higher solubilization of RVT in the lipid, thereby ensuring less RVT available for partitioning into the aqueous phase. Besides, an increase in the lipid content increases the viscosity of the lipid phase, which in turn helps in quicker solidification of lipid, thereby giving little time for the drug to diffuse out of the lipid (Hao et al., 2011). As the surfactant concentration increases, the % EE was found to reduce. The increase in the surfactant increases the solubilization of RVT in the aqueous phase, subsequently leading to an increase in the partitioning of RVT from lipid phase to aqueous phase, which was also reported in other studies (Khalil et al., 2013). We observed a negative effect of the drug (%) on % EE, which may be due to the lack of enough lipid molecules present to solubilize RVT completely in lower lipid content and thereby increase the partitioning of RVT into the aqueous phase (Thatipamula et al., 2011). Among all the independent variables, the total lipid showed a major impact on the % EE of RVT into the NLCs as observed from the F value. The regression equation for % EE, presenting the significant factors is shown in Eq. (4).

$$\%\ EE = -66.4 + 2.571\,[Total\ lipid] - 1.5\,[Surfactant] - 0.69\,[Drug] - 0.01356\,[Total\ lipid*Total\ lipid] - 13.58\,[Surfactant\ *Surfactant] + 0.360\,[Total\ lipid*Surfactant] - 1.626\,[Surfactant\ *Drug] \quad (4)$$

The three-dimensional (3D) surface plots give us a visual observation of the obtained results. The factors that have shown a major impact on the critical variables were considered for constructing the 3D surface plots and are presented in Fig. 5. Fig. 5a presents the effect of total lipid and surfactant concentration on the particle size. As evident from the plot, the particle size increases with an increase in the total lipid and a reduced surfactant concentration. PDI of the formulation decreased with the increase in the surfactant concentration and decreased total lipid concentration (Fig. 5b). The zeta potential was found to decrease as the oil (%) increases; however, total lipid concentration did not influence the zeta potential (Fig. 5c). The EE of NLCs increased with an increase in the total lipid and a decrease in the surfactant concentration (Fig. 5d).

The desirability plot was generated using the software by giving the input of the upper and lower limits of the desired responses. The predicted values for the variables, which would help in achieving the desired responses were noted down. A composite desirability value of 0.9075 was obtained. The suitability of the software-predicted runs was assessed by performing the experimental runs and then comparing the results obtained by the software. The results are presented in Table 5. The results showed a closeness with the predicted results evident from the lower error. This demonstrates that the formulation parameters suggested by the software hold well from an experimental point of view. Fig. 6 shows the desirability plot for the optimized formulation (RVT-

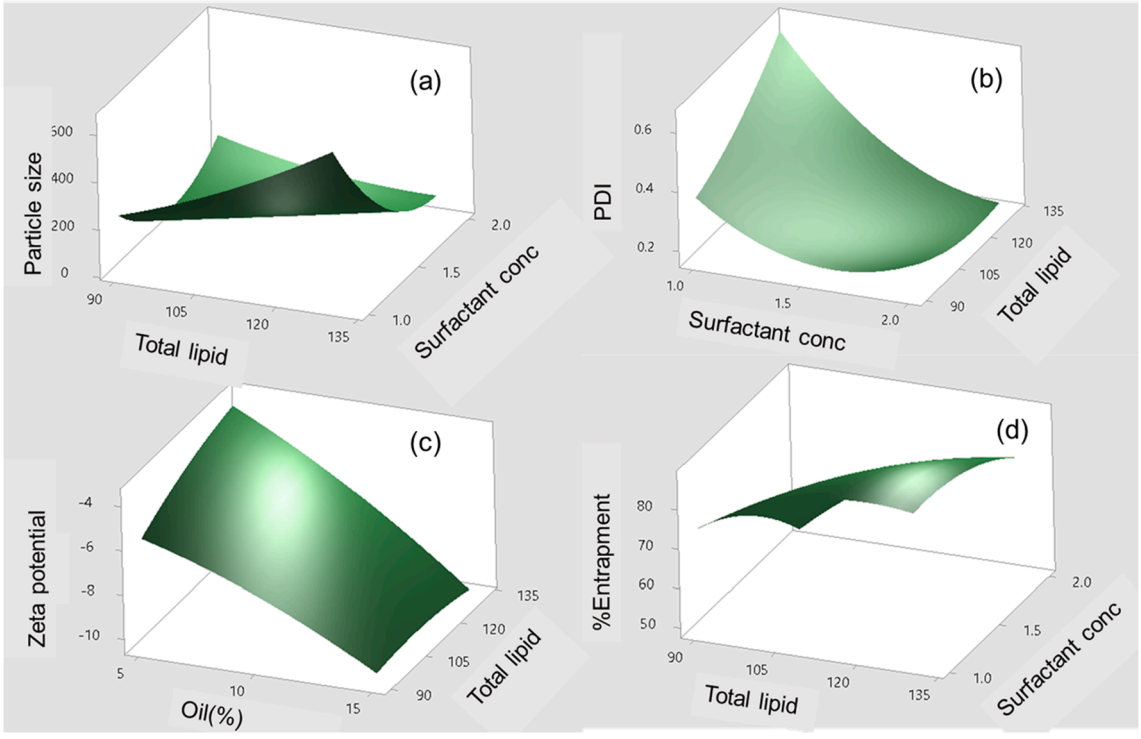

Fig. 5. Three-dimensional surface plots of (a) Particle size *vs.* total lipid, surfactant concentration, (b) Polydispersity index (PDI) *vs.* surfactant concentration, total lipid, (c) Zeta potential *vs.* oil (%), total lipid, (d) Entrapment efficiency *vs.* surfactant concentration, total lipid.

Table 5
Predicted and observed responses for the optimized formulation and evaluation of the sensitivity of the design space.

Response	Predicted value	Observed	% Error*
Software suggested solution for optimized formulation (RVT-NLCs)			
Particle size (nm)	102.37	104.47 ± 4.35	2.05
Polydispersity index	0.19	0.19 ± 0.02	3.61
Zetapotential (mV)	−10.51	−9.81 ± 0.75	6.66
Entrapment efficiency (%)	78.91	77.57 ± 1.06	1.70
Flagged region-1			
Particle size (nm)	79.20	79.65 ± 4.13	0.57
Polydispersity index	0.18	0.18 ± 0.09	0.55
Zeta potential (mV)	−10.37	−10.39 ± 2.99	0.19
Entrapment efficiency (%)	75.61	74.63 ± 1.18	1.30
Flagged region-2			
Particle size (nm)	83.16	87.57 ± 3.82	5.30
Polydispersity index	0.21	0.20 ± 0.01	5.31
Zetapotential (mV)	−10.11	−9.41 ± 3.98	6.92
Entrapment efficiency (%)	70.02	69.54 ± 0.52	0.68
Flagged region-3			
Particle size (nm)	159.76	156.90 ± 6.70	1.79
Polydispersity index	0.25	0.24 ± 0.03	2.02
Zetapotential (mV)	−9.95	−10.27 ± 1.31	3.22
Entrapment efficiency (%)	79.94	79.25 ± 1.40	0.86

* % Error = (Predicted results − observed results)/Predicted results × 100.

NLCs).

3.2.3. Establishment and validation of the design space

The overlay contour plot generated to establish the design space is presented in Fig. 6. It provides a range within which we can expect the desired responses in a study. The plot was obtained by applying constraints on the desired responses. Two factors, namely total lipid and surfactant concentration were included, and the rest of the factors, oil (%) and drug (%) were kept at hold values corresponding to that of the optimized formulation.

The design space analysis is important from a scale-up point of view to assess the robustness of the generated design space. The software suggested values within the design space, as well as in and around it was compared with the experimental results (Table 5). The flagged region-1 represents the design space, flagged region-2 is the one on the boundary line of the design space, and flagged region-3 falls outside the design space generated (Fig. 7). The regions outside the design space are those where any one of the responses will be either lower or higher than desired. The results suggest that the design space was found to be sensitive to changes in the independent variables when formulations were developed as per the conditions mentioned beyond the design space. Nevertheless, any area within the design space showed similar results as that predicted, suggesting the robustness of the design space.

3.3. Characterization of the NLCs formulation

3.3.1. Surface morphology by TEM

The prepared RVT-NLCs were visualized using TEM (Fig. 8A). NLCs were spherical with a smooth and regular surface, and size distribution was found to be uniform, and there was no visible aggregation of RVT-NLCs.

3.3.2. DSC analysis

As shown in Fig. 8B, the DSC thermogram for pure RVT revealed a sharp melting endotherm at 269.86 °C. The physical mixture of RVT with GMS showed two endothermic peaks at 264.04 °C and 74.51 °C corresponding to RVT and GMS, respectively. The absence of the melting endotherm corresponding to RVT in the thermogram of RVT-NLCs indicated the encapsulation and transformation of RVT into amorphous form in the NLCs formulation.

3.3.3. Powder X-ray diffraction studies

The powder X-ray diffractogram of pure RVT showed intense Bragg peaks at 2θ values of 6.45°, 16.32°, 18.91°, and 28.04° indicating its crystalline nature. In the placebo NLCs, two peaks were observed at 19.75° and 22.99°. However, in RVT-NLCs, the absence of intense peaks corresponding to RVT suggested the conversion of RVT into its amorphous form when encapsulated within the solid and liquid lipid matrix of NLCs (Fig. 8C) (Vijayakumar et al., 2016; Zu et al., 2014). This result was supported by the DSC analysis as discussed in Section 3.3.2.

3.3.4. FT-IR analysis

In the FT-IR spectra (Fig. 8D), RVT showed characteristic peaks at 3292.49 cm^{-1} (–OH stretching), 1382.96 (phenyl –OH bending), 1151.50 cm^{-1} (C-O stretching), 1591.27 cm^{-1} to 1452.40 cm^{-1} (aromatic C = C stretching), 3024.38 cm^{-1} (C-H stretching for alkene), 2889.37 cm^{-1} (C-H stretching for alkane), and 977.91 cm^{-1} (disubstituted C = C trans alkene bending) (Jose et al., 2014). All the characteristic peaks of RVT were present in the optimized NLCs formulation (RVT-NLCs), thus demonstrating that there was no significant change in the RVT functional groups in the NLCs formulation.

3.3.5. Evaluation of RVT-NLCs incorporated into carbopol

The optimized RVT-NLCs were incorporated into carbopol 934 (CP) as a thickener. The RVT-NLCs-CP was found to be whitish with homogenous consistency when observed visually. The viscosity of the gel was found to be 6,845 ± 6.32 cps at 25 °C.

3.3.6. In vitro release profile

The *in vitro* release profile from the RVT-NLCs and RVT-NLCs-CP is shown in Fig. 9. We observed 72.82 ± 9.24% and 84.80 ± 5.42% of drug release from the RVT-NLCs and 51.81 ± 6.31% and 83.79 ± 4.01% of drug release from RVT-NLCs-CP at the end of 12 h and 48 h, respectively. An initial burst release of RVT from RVT-NLCs was observed, which may have occurred due to the RVT present on the surface of NLCs. Following this, a sustained release was observed, which may be attributed to the slow diffusion of RVT from the core of the NLCs as reported in literatures (Poonia et al., 2019; Rute Neves et al., 2013). The release of RVT from RVT-NLCs-CP was slower till 12 h when compared to that from RVT-NLCs. This may be due to the time taken for RVT to diffuse out of the carbopol matrix. The data obtained for RVT-NLCs were fitted into zero-order, first-order, Higuchi and Korsmeyer-Peppas models to predict the release kinetics and mechanism of RVT release. The release from RVT-NLCs was found to follow the Higuchi model with an $R^2 = 0.839$. The *n* value obtained from the Korsmeyer-Peppas model was found to be 0.831, suggesting an anomalous transport of RVT from NLCs matrix indicating that the drug release is controlled by more than one process, coupling of diffusion controlled and erosion mechanism. A smaller sized particle releases the drug faster than that compared to larger size particles due to its higher surface area and shorter diffusion path. During the process of melt emulsification method, due to the saturation solubility, drug gets partitioned into the aqueous phase at high temperature, and during further cooling, repartitioning into the lipid phase takes place. A solid core starts forming at the recrystallization temperature and the crystallized core is no longer available for repartitioning of the drug, hence drug concentration will be higher near the surface of a particle than compared to its core, which is the main reason for the initial burst release of drug (Chen et al., 2017; Duong et al., 2019; Khosa

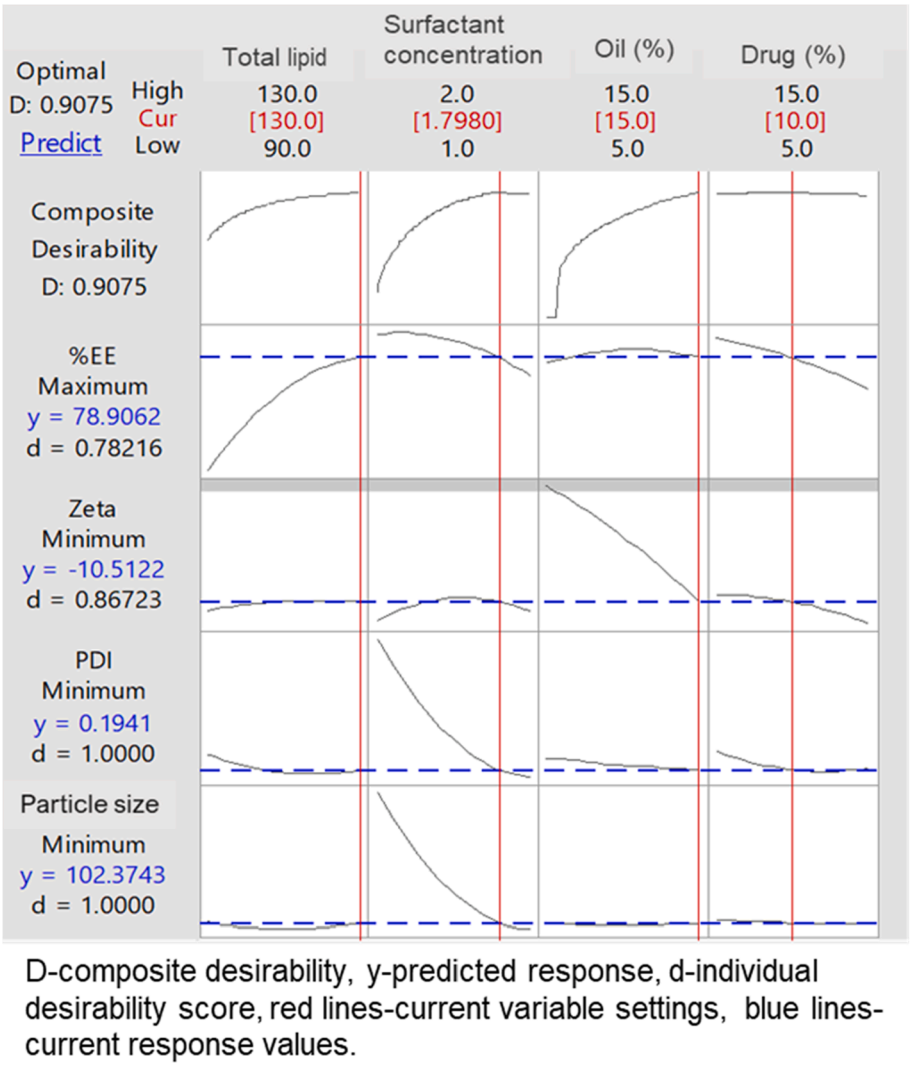

Fig. 6. Desirability plot for the optimized NLCs formulation.

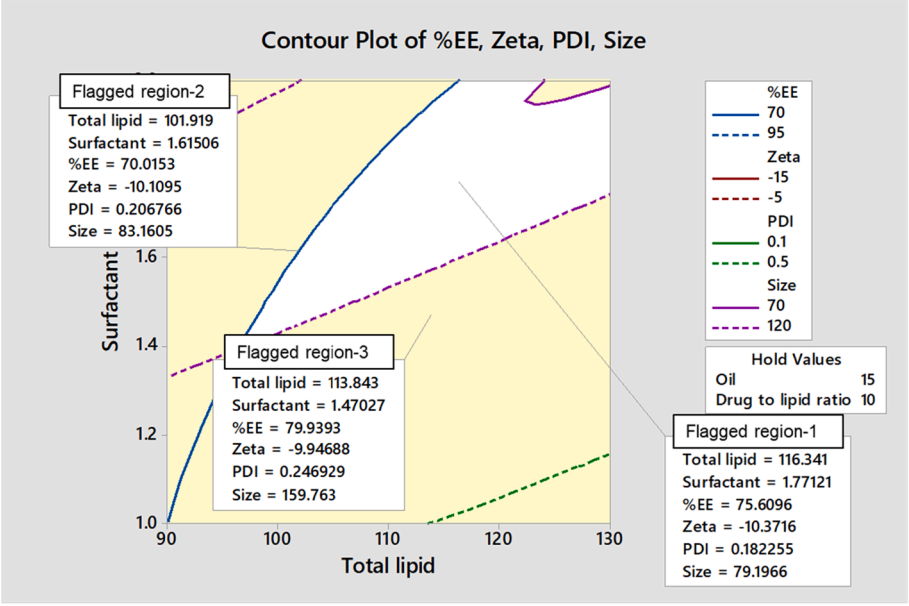

Fig. 7. Overlay contour plot indicating the design space.

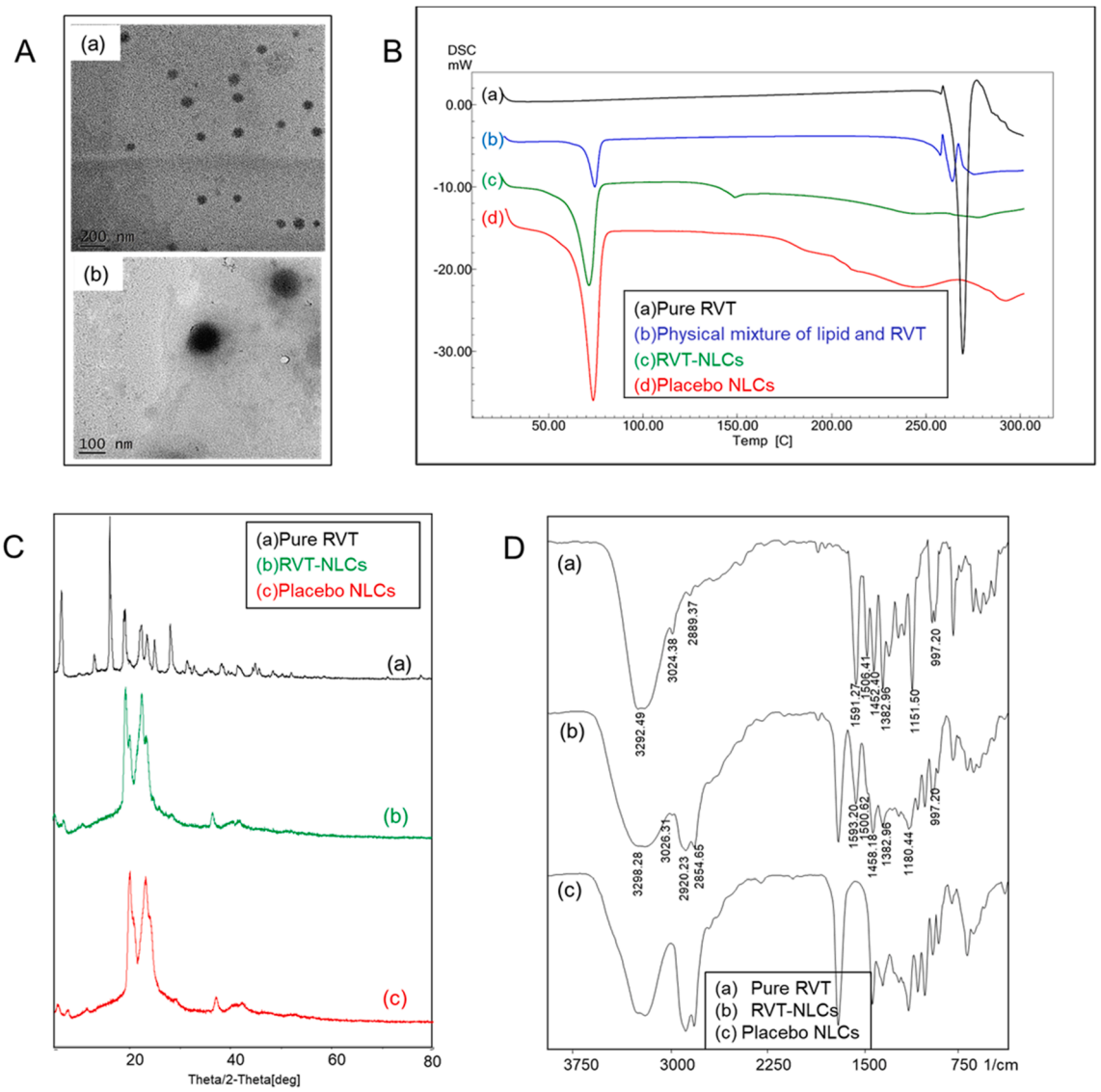

Fig. 8. (A) TEM images of RVT-NLCs at scale bar of (a) 200 nm and (b) 100 nm, (B) DSC thermograms (C) Powder X-ray diffractogram and (D) FT-IR spectra of pure RVT and formulations.

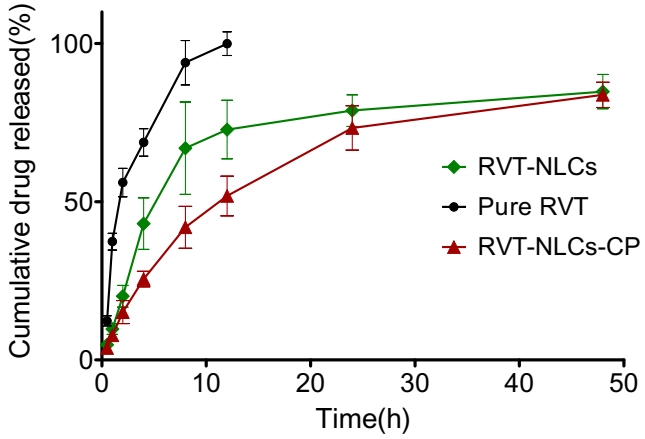

Fig. 9. Drug release profile of RVT loaded formulations.

et al., 2018; Nagaich and Gulati, 2016; Zur Mühlen et al., 1998).

3.3.7. *Skin permeation study using MN*

The MN provides minimally invasive quick onset of action much like hypodermic needle (Halder et al., 2020). The main rationale to use MN is to provide high concentration of drug around the site of application locally. Bores in the microneedles provides an effective means of delivery for local drug absorption which may otherwise not be possible only with NLCs. MN enables the delivery and diffusion of the NLCs into a wide area continuously through the MN bores. Moreover, the lipophilic nature of NLCs helps in creating depot of drug (Raghu Nandan Reddy, 2012) which will distribute into the nearby adipose tissue in the breast and helps to maintain high drug concentration at the breast tissue and very little amount of drug will be released into the blood stream in a controlled manner.

In this study, hollow microneedle array was used for the delivery of intact NLCs. Coated microneedles cannot be used for the NLCs loading as it is difficult to achieve the efficient coating of NLCs and release of intact NLCs. Another reason behind using microneedle array system instead of loading the drug within the MN is to provide flexibility for dose adjustment, to suit the patient requirement. Davis et al. (2005) have

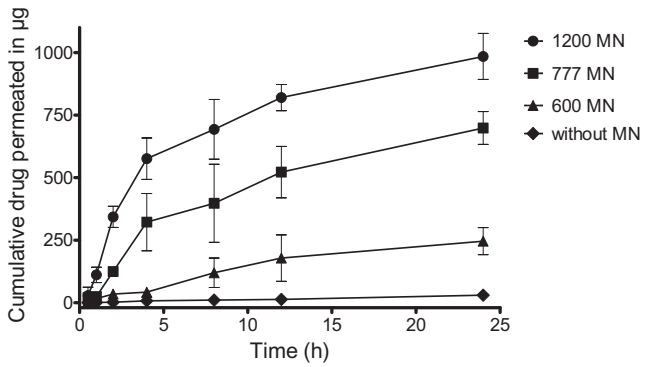

Fig. 10. Skin permeation profile of RVT-NLCs-CP using needle 1200 MN, 777 MN, and 600 MN having a length of 1100 µm, 700 µm, and 500 µm with 43, 121, and 187 number of needles per $cm^{2.}$

used microneedle arrays for the efficient delivery of insulin and obtained promising results (Davis et al., 2005). In one of our previous works, we have successfully delivered donepezil loaded niosomes to the brain with the help of similar MN arrays (Nayak et al., 2020).

MN array systems used in the experiment had a diameter of 1 cm^2, with variation in needle number and length. The needles 1200 MN, 777 MN, and 600 MN had a length of 1100 µm, 700 µm, and 500 µm with 43, 121, and 187 needles per cm^2 respectively. The results of the skin permeation study revealed that the 1200 MN showed maximum permeation and flux as compared to that without MN as well as other MN array systems, with the order of permeation 1200 MN > 777 MN > 600 MN > without MN (Fig. 10). The maximum permeation ability of the 1200 MN array system may be due to the higher needle length as compared to other MN array systems. Although the 600 MN array system had the highest needle number per cm^2, it showed lower permeation than 1200 MN. It was evident that permeation increases with the length of the needles, irrespective of the number of needles per cm^2. The 1200 MN reaches deep into the dermis, the deeper region of the dermis consists of a network of blood vessels, this might be the reason why it has shown lower skin retention compared with other MN arrays (Fernandes, 2017). 1200 MN has a fewer number of needles, hence a lesser number of cuts on the skin, thereby leading to less amount of drug diffusion in the horizontal direction into the skin. The studies carried out without MN showed maximum skin retention which may be due to the stratum corneum's higher lipidic nature which may hold and prevent the NLCs from crossing the skin (Viegas et al., 2020). A 32.8 fold increase in the permeation was observed using 1200 MN compared to that without the MN. Based on the results, we concluded that the 1200 MN array system could maintain the required flux of RVT to achieve the therapeutic concentration. Table 6 presents the data for the cumulative RVT permeated, the flux of RVT across the skin, and its retention in the skin at the end of 24 h.

Table 6
Skin permeation data using 1200 MN, 777 MN, and 600 MN having needle length of 1100 µm, 700 µm, and 500 µm with 43, 121, and 187 number of needles per cm^2.

MN array system	Cumulative drug permeated at the end of 24 h (µg) Mean ± SD	Flux (µg/cm^2/h) Mean ± SD	RVT retention in the skin at the end of 24 h (µg) Mean ± SD
MN1200	984.69 ± 91.70	37.44 ± 6.22	15.60 ± 8.75
MN777	698.43 ± 65.57	28.75 ± 3.87	24.33 ± 4.69
MN600	246.12 ± 54.03	10.62 ± 1.43	26.51 ± 6.43
Without MN	30.01 ± 4.30	1.21 ± 0.07	32.42 ± 8.56

3.4. Accelerated stability studies

The stability of RVT-NLCs-CP was assessed at 5 ± 3 °C and 25 ± 2 °C/60 ± 5% relative humidity (RH) for four months period (Manikkath et al., 2020). The samples were analyzed after the 2nd and 4th months for viscosity, drug content, and % release of RVT. The viscosity of the formulation did not show any significant change during the stability study period. The samples kept at 5 ± 3 °C showed around 3 % reduction in the assay value at the end of 4th month. However, the samples stored at 25 °C ± 2 °C/60% RH ± 5% RH showed around 5% decrease in the assay value at the end of 2nd month and about 7% reduction in assay value at the end of 4th month, which may be due to the degradation of RVT (Table 7). The % release of RVT from the formulation did not change during the stability study period (Kosović et al., 2020; Nagaich and Gulati, 2016).

3.5. Cell cytotoxicity assay

The MDA-MB-231 cell viability profile on treatment with RVT and RVT- NLCs is shown in Fig. 11. The IC_{50} values are shown in Table 8. The IC_{50} of the RVT-NLCs was found to be lower than that of pure RVT, indicating that RVT-NLCs are comparatively more potent than the free RVT. Reports suggest that NLCs can undergo cellular internalization due to their cancer cell affinity owing to their bioadhesive feature and fusion with the cell membrane (Chand et al., 2021). The higher penetration of RVT-NLCs due to their higher lipophilic nature and slow release of RVT from NLCs may be the possible reason for their effective and prolonged anticancer activity compared to pure RVT. The placebo NLCs did not show any toxic effect on the cell lines, clearly indicating that the cytotoxicity of the RVT-NLCs is not due to the carrier by itself (Nordin et al., 2019).

3.6. Cellular uptake study

The results of the study revealed that in MDA-MB-231 cell lines, a significant amount of uptake of FITC-NLCs was observed. We observed that there was no significant uptake of NLCs at 1 h and 2 h. However, at 4 h and 6 h, we were able to observe a significant amount of NLCs uptake. We observed that some of the NLCs have adhered to the membrane, which may be due to the lipophilic nature of the NLCs (Fig. 12).

3.7. Cell migration assay

The cell migration assay was performed for 24 h after scratching the

Table 7
Data for accelerated stability studies.

Time intervals	Conditions	Viscosity (cps)	Drug content (%)	% drug release at the end of 48 h
Initial	5 ± 3 °C	6809 ± 8.50	99.56 ± 2.91	84.67 ± 5.67
	25 °C ± 2 °C/60% RH ± 5% RH	6978 ± 12.64	98.93 ± 2.06	85.23 ± 4.82
2 months	5 ± 3 °C	6782 ± 10.22	98.85 ± 3.05	82.98 ± 6.75
	25 °C ± 2 °C/60% RH ± 5% RH	6964 ± 17.03	93.21 ± 5.87	86.01 ± 4.52
4 months	5 ± 3 °C	6868 ± 8.63	96.32 ± 3.81	83.44 ± 6.31
	25 °C ± 2 °C/60% RH ± 5% RH	6772 ± 18.06	91.80 ± 6.64	85.61 ± 5.23

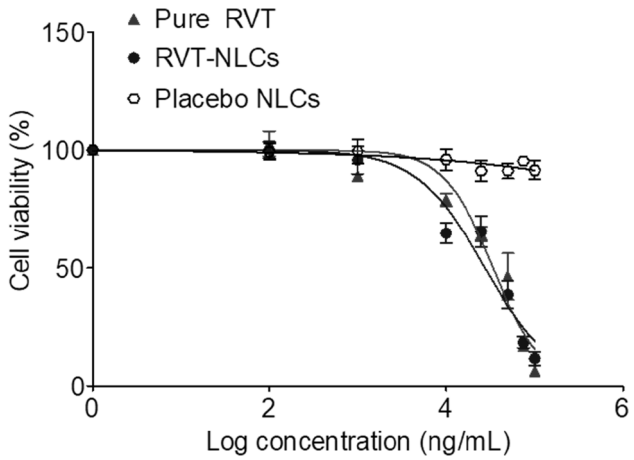

Fig. 11. Cell viability analysis using alamarBlue assay on MDA-MB-231 cell lines.

Table 8
Comparison of IC_{50} values of RVT-NLCs with pure drug.

Cell lines	Sample	IC_{50} (μg/mL)Mean ± SD (n = 3)
MDA-MB-231	Pure RVT	33.93 ± 7.34
	RVT-NLCs	27.50 ± 3.43

cell monolayer. The images were taken at intervals of 0 h, 16 h, and 24 h (Fig. 13). In the control group and the group treated with placebo NLCs, we observed a complete wound closure at 24 h, suggesting that the NLCs as carrier played no role in the inhibition of cell migration. In the cells treated with the pure RVT and RVT-NLCs, minimum cell migration was observed for the study duration (24 h) compared to the initial scratch distance. Significant inhibition of wound closure was observed in both the pure RVT and RVT-NLCs group ($p < 0.05$) when compared with the control and placebo NLCs groups, demonstrating the cell migration inhibitory property of RVT and RVT-NLCs.

3.8. Pharmacokinetic and tissue distribution studies

The pharmacokinetic parameters of the developed MN array transdermal drug delivery system were compared with the single dose of pure RVT given orally and RVT-NLCs-CP via s.c. route in Sprague Dawley rats. The concentration of RVT in the plasma after a single oral dose, and RVT-NLCs-CP via MN and s.c. administration is presented in Fig. 14(a) and pharmacokinetic parameters are summarized as mean ± SD in Table 9. C_{max} was significantly increased in MN when compared with the pure drug given orally. RVT-NLCs-CP given via MN showed a significant rise in the $AUC_{0\text{-}t}$ when compared with the pure drug as well as RVT-NLCs-CP given s.c, demonstrating an increase in the bioavailability. Increase in this $AUC_{0\text{-}t}$ and C_{max} for RVT-NLCs-CP via MN could be attributed to the avoidance of the first-pass metabolism reported for RVT when given orally. There was a delay in reaching the T_{max} in the MN group when compared with oral and s.c. group indicating a sustained release of RVT from the carrier or more time taken by the NLCs to reach the bloodstream when administered via MN. A higher value of MRT and lower value of Ke of RVT-NLCs-CP via MN over oral pure RVT and s.c. administration of RVT-NLCs-CP confirms the longer retention of RVT in the blood stream when administered via MN. In the s.c group C_{max} of 1251.02 ± 93.34 ng/mL reached at 0.25 ± 0.07 h whereas a C_{max} of 343.75 ± 31.89 ng/mL reached at 2 h in the MN group, indicating a rapid rise in the RVT plasma concentration followed by its drastic reduction with higher elimination rate in the s.c. group, whereas MN group showed steady-state release phase of RVT with lower elimination rate. Moreover, in the s.c treated animals, after 12 h, the RVT in the

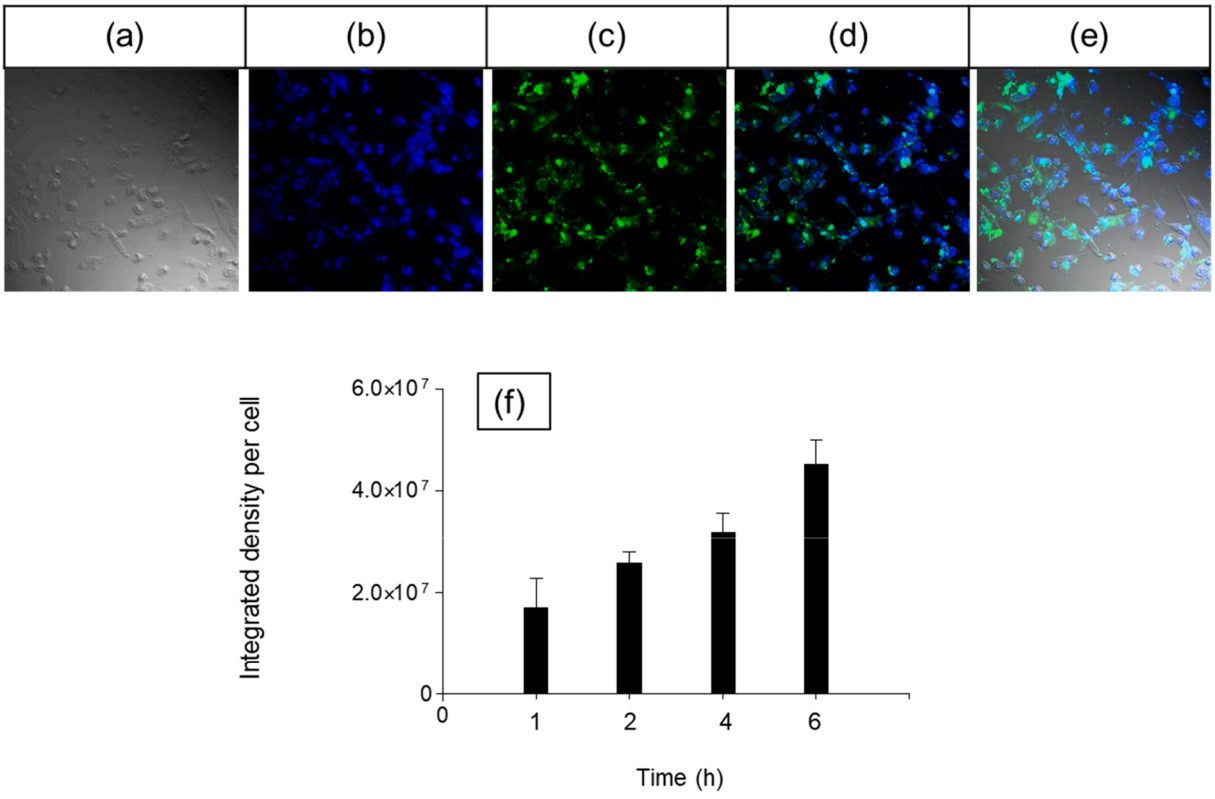

Fig. 12. Cellular uptake of FITC-NLCs (6 h) (a) bright-field image, (b) Hoechst-stained nuclei of the cells, (c) FITC-NLCs uptake, (d) overlay of images (b) and (c), (e) overlay of images (a), (b) and (c). (f) Profile of fluorescence intensity/cell (a.u.) of MDA-MB-231 (the error is represented as SD).

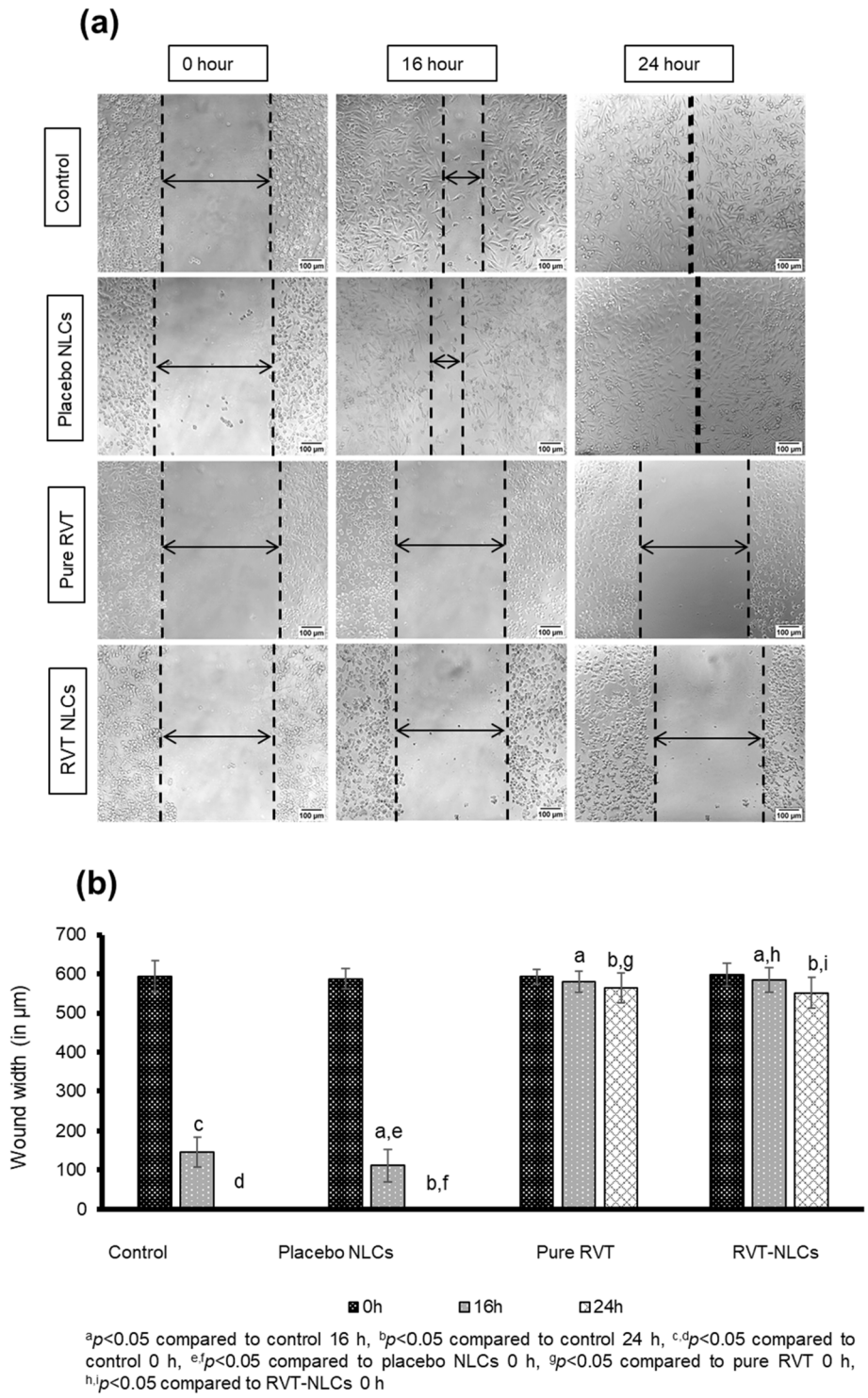

Fig. 13. *In vitro* cell migration assay (a) images and (b) quantitative representation of wound width at 0, 16, and 24 h after incubation (n = 3, and data is presented in terms of mean ± SD).

plasma could hardly be measured, whereas in that using MN, quite good amount of RVT at the end of 24 h was observed, indicating an extended release of RVT which may thereby reduce the dosing frequency. The significantly higher MRT and lower Ke of RVT-NLCs-CP via MN over oral pure RVT and s.c. administration of RVT-NLCs-CP further evidenced the sustained release characteristics of RVT incorporated in NLCs when administered via MN. Similar trend of results were obtained by Ramöller and coworkers in their study (Ramöller et al., 2019).

Fig. 14(b) represents the RVT concentration profile at different time intervals when treated with RVT-NLCs-CP using MN in the breast tissue. Higher retention of RVT in the breast tissue compared to plasma was observed (at all the time points) indicating the localized/ site-specific delivery of the RVT-NLCs. This may be due to the high lipophilic nature of the NLCs and RVT. However, when pure RVT was administered orally, a negligible amount of RVT was detected (68 ng/mL) at 0.3 h and no response was detected at subsequent time points in the breast tissue (Data not shown). The pharmacokinetics parameters calculated for RVT-NLCs in the breast tissue demonstrated a significantly higher C_{max}, T_{max},

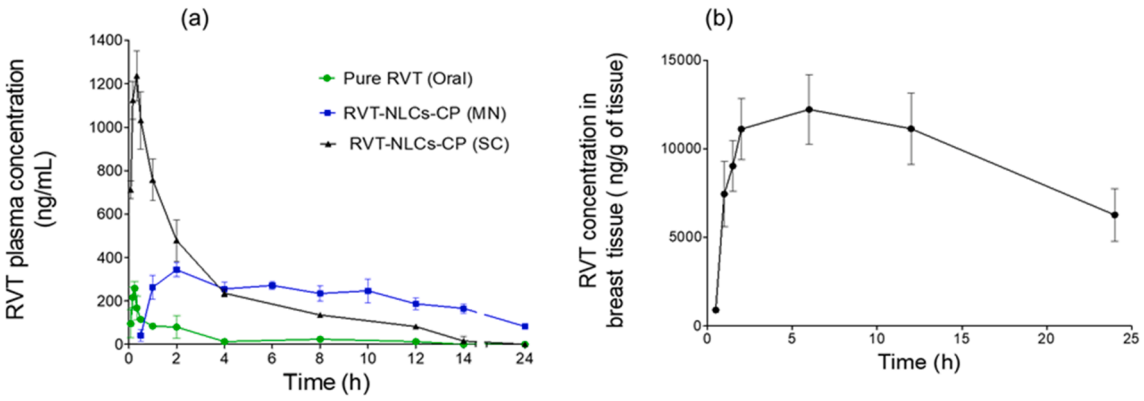

Fig. 14. (a) Plasma-concentration time profile for pure RVT (oral) subcutaneous administration of RVT-NLCs-CP, and MN assisted RVT-NLCs-CP, (b) Concentration time profile of RVT in breast tissue after MN assisted RVT-NLCs-CP delivery.

Table 9
Pharmacokinetic parameters for pure RVT and RVT-NLCs-CP in plasma and breast tissue.

Parameters	Pharmacokinetics			Breast tissue distribution
	Pure RVT (p.o.)	RVT-NLCs-CP (SC)	RVT-NLCs-CP (MN)	RVT-NLCs-CP (MN)
C_{max}(ng/mL)	269.30 ± 30.26	1251.02 ± 93.34	343.75 ± 31.89^{*+++}	12230.6 ± 1953.45$^{\#\#\#}$
T_{max}(h)	0.3 ± 0.0	0.25 ± 0.07	2.0 ± 0.0^{***+++}	6.0 ± 0.0$^{\#\#\#}$
$t_{1/2}$(h)	3.81 ± 0.85	1.35 ± 0.06	9.98 ± 0.27**	14.41 ± 1.41$^{\#\#}$
Ke (1/h)	0.18 ± 0.04	0.52 ± 0.03	0.07 ± 0.002^{**+++}	0.05 ± 0.005$^{\#\#\#}$
$AUC_{0\text{-}t}$ (h*ng/mL)	458.3 ± 21.21	3590.65 ± 122.97	4529.2 ± 299.67^{***+++}	234128.3 ± 42789.86$^{\#\#\#}$
$AUC_{0\text{-}inf}$ (h*ng/mL)	532.8 ± 79.97	3647.3 ± 122.05	5716.95 ± 396.90^{***+++}	366075.8 ± 86372.81$^{\#\#\#}$
$MRT_{0\text{-}t}$(h)	5.7 ± 0.14	5.55 ± 0.21	15.7 ± 1.48^{***++}	22.95 ± 2.05$^{\#\#\#}$

Statistically significant at $^{*}p < 0.05$, $^{**}p < 0.01$, $^{***}p < 0.001$ when compared to oral plasma concentration of RVT, $+p < 0.05$, $++p < 0.01$, $+++p < 0.001$ when compared to SC plasma concentration of RVT, and $\#p < 0.05$, $\#\#p < 0.01$, $\#\#\#p < 0.001$ when compared to MN plasma concentration.

and $AUC_{0\text{-}t}$ compared to that in the plasma (Table 9). These results further substantiated that MN-assisted RVT-NLCs-CP successfully enhanced the localized delivery of RVT to the breast tissue.

4. Conclusion

In the present work, NLCs formulations of RVT were successfully developed for the local transdermal delivery via a microneedle array system to the breast tissue. The NLCs were optimized using statistical models that demonstrated optimum particle size, PDI, zeta potential, and drug entrapment. The formulations were found to be stable for the duration of storage up to four months. The RVT-NLCs enhanced the transdermal permeation of RVT significantly via MN array systems with less skin retention than that without MN. Of the different MN array systems tried, 1200 MN array systems showed the highest flux of RVT. The cell viability studies revealed greater cytotoxicity of RVT-NLCs compared to pure RVT. The cellular uptake studies revealed enhanced cellular uptake of NLCs. Moreover, the pharmacokinetic profile of the formulations was improved when administered via MN array system as compared to the oral route. The tissue distribution studies showed promising results of localized concentration of the formulation in the breast tissue. Hence, the developed RVT-NLCs when combined with the advantage of MN arrays may enhance the bioavailability and localized effect of RVT, thereby showing a better therapeutic outcome in breast cancer. The developed NLCs can further enable the prolonged release of RVT thereby reducing the dosing frequency and improving patient compliance.

CRediT authorship contribution statement

Shivaprasad Gadag: Conceptualization, Data curation, Formal analysis, Methodology, Validation, Visualization, Writing - original draft. **Reema Narayan:** Methodology, Validation, Data curation, Writing - review & editing. **Archana S. Nayak:** Resources. **Diana Catalina Ardila:** Formal analysis, Writing - review & editing. **Shilpa Sant:** Formal analysis, Funding acquisition, Supervision, Project administration, Visualization, Writing - review & editing. **Yogendra Nayak:** Supervision, Writing - review & editing. **Sanjay Garg:** Supervision, Writing - review & editing. **Usha Y. Nayak:** Conceptualization, Data curation, Funding acquisition, Investigation, Methodology, Project administration, Resources, Supervision, Validation, Visualization, Writing - review & editing.

Declaration of Competing Interest

The authors declare that they have no known competing financial interests or personal relationships that could have appeared to influence the work reported in this paper.

Acknowledgements

The authors are thankful to Manipal College of Pharmaceutical Sciences, Manipal Academy of Higher Education, Manipal, India for providing the necessary facilities for the research work, and to DST-SAIF, Cochin, India for TEM analysis. We are grateful to Ms. Tianling Hou for the training on the handling of cell lines.

Funding

This project was supported by the Science and Engineering Research Board, Dept. of Science and Technology, New Delhi, India (EMR/2016/007006). This work is also supported by the National Institute of Health (NIH R37CA232209) award to Dr Shilpa Sant.

References

Al-malah, K., 2014. Rheological Properties of Carbomer Dispersions Rheological Properties of Carbomer Dispersions.

Bhatnagar, S., Bankar, N.G., Kulkarni, M.V., Venuganti, V.V.K., 2019. Dissolvable microneedle patch containing doxorubicin and docetaxel is effective in 4T1 xenografted breast cancer mouse model. Int. J. Pharm. 556, 263–275. https://doi.org/10.1016/j.ijpharm.2018.12.022.

Bhatnagar, S., Kumari, P., Pattarabhiran, S.P., Venuganti, V.V.K., 2018. Zein microneedles for localized delivery of chemotherapeutic agents to treat breast cancer: drug loading, release behavior, and skin permeation studies. AAPS PharmSciTech 19, 1818–1826. https://doi.org/10.1208/s12249-018-1004-5.

Bishayee, A., 2009a. Cancer prevention and treatment with resveratrol: from rodent studies to clinical trials. Cancer Prev. Res. 2, 409–418. https://doi.org/10.1158/1940-6207.CAPR-08-0160.

Bishayee, Anupam, 2009. Cancer prevention and treatment with resveratrol: From rodent studies to clinical trials. Cancer Prev. Res. https://doi.org/10.1158/1940-6207.CAPR-08-0160.

Bohrey, S., Chourasiya, V., Pandey, A., 2016. Polymeric nanoparticles containing diazepam: preparation, optimization, characterization, in-vitro drug release and release kinetic study. Nano Converg. 3, 3. https://doi.org/10.1186/s40580-016-0061-2.

Bonnier, F., Keating, M.E., Wróbel, T.P., Majzner, K., Baranska, M., Garcia-Munoz, A., Blanco, A., Byrne, H.J., 2015. Cell viability assessment using the Alamar blue assay: A comparison of 2D and 3D cell culture models. Toxicol. Vitr. 29, 124–131. https://doi.org/10.1016/j.tiv.2014.09.014.

Carter, L.G., D'Orazio, J.A., Pearson, K.J., 2014. Resveratrol and cancer: Focus on in vivo evidence. Endocr. Relat. Cancer. https://doi.org/10.1530/ERC-13-0171.

Ch, L., Hc, C., Wc, W., Sl, S., Cy, H., 2014. Novel lutein loaded lipid nanoparticles on porcine corneal distribution. J. Ophthalmol. 2014 https://doi.org/10.1155/2014/304694.

Chand, P., Kumar, H., Badduri, N., Gupta, N.V., Bettada, V.G., Madhunapantula, S.R.V., Kesharwani, S.S., Dey, S., Jain, V., 2021. Design and evaluation of cabazitaxel loaded NLCs against breast cancer cell lines. Colloids Surf. B Biointerfaces 199. https://doi.org/10.1016/j.colsurfb.2020.111535.

Chedea, V.S., Vicaş, S.I., Sticozzi, C., Pessina, F., Frosini, M., Maioli, E., Valacchi, G., 2017. Resveratrol: From diet to topical usage. Food Funct. https://doi.org/10.1039/c7fo01086a.

Chen, W., Palazzo, A., Hennink, W.E., Kok, R.J., 2017. Effect of particle size on drug loading and release kinetics of gefitinib-loaded PLGA microspheres. Mol. Pharm. 14, 459–467. https://doi.org/10.1021/acs.molpharmaceut.6b00896.

Chen, X., He, H., Wang, G., Yang, B., Ren, W., Ma, L., Yu, Q., 2007. Stereospecific determination of cis- and trans-resveratrol in rat plasma by HPLC: Application to pharmacokinetic studies. Biomed. Chromatogr. 21, 257–265. https://doi.org/10.1002/bmc.747.

Cho, S., Namkoong, K., Shin, M., Park, J., Yang, E., Ihm, J., Thu, V.T., Kim, H.K., Han, J., 2017. Cardiovascular protective effects and clinical applications of resveratrol. J. Med. Food. https://doi.org/10.1089/jmf.2016.3856.

Cragg, G.M., Pezzuto, J.M., 2016. Natural Products as a Vital Source for the Discovery of Cancer Chemotherapeutic and Chemopreventive Agents, in: Medical Principles and Practice. S. Karger AG, pp. 41–59. https://doi.org/10.1159/000443404.

Davis, S.P., Martanto, W., Allen, M.G., Prausnitz, M.R., 2005. Hollow metal microneedles for insulin delivery to diabetic rats. IEEE Trans. Biomed. Eng. 52, 909–915. https://doi.org/10.1109/TBME.2005.845240.

Duong, V.A., Nguyen, T.T.L., Maeng, H.J., Chi, S.C., 2019. Data on optimization and drug release kinetics of nanostructured lipid carriers containing ondansetron hydrochloride prepared by cold high-pressure homogenization method. Data Br. 26 https://doi.org/10.1016/j.dib.2019.104475.

Emami, J., Mohiti, H., Hamishehkar, H., Varshosaz, J., 2015. Formulation and optimization of solid lipid nanoparticle formulation for pulmonary delivery of budesonide using Taguchi and Box-Behnken design. Res. Pharm. Sci. 10, 17–33.

Farooq, M.A., Li, L., Parveen, A., Wang, B., 2019. Globular protein stabilized nanoparticles for delivery of disulfiram: Fabrication, characterization,: In vitro toxicity, and cellular uptake. RSC Adv. 10, 133–144. https://doi.org/10.1039/c9ra09468g.

Fernandes, D., 2017. Commentary on: micro-needling depth penetration, presence of pigment particles, and fluorescein-stained platelets: clinical usage for aesthetic concerns. Aesthetic Surg. J. 37, 86–88. https://doi.org/10.1093/asj/sjw151.

Gadag, S., Sinha, S., Nayak, Y., Garg, S., Nayak, U.Y., 2020. Combination therapy and nanoparticulate systems: Smart approaches for the effective treatment of breast cancer. Pharmaceutics. https://doi.org/10.3390/pharmaceutics12060524.

Gokce, E.H., Korkmaz, E., Dellera, E., Sandri, G., Cristina Bonferoni, M., Ozer, O., 2012. Resveratrol-loaded solid lipid nanoparticles versus nanostructured lipid carriers: Evaluation of antioxidant potential for dermal applications. Int. J. Nanomedicine 7, 1841–1850. https://doi.org/10.2147/IJN.S29710.

Gu, X., Zhang, W., Liu, J., Shaw, J.P., Shen, Y., Xu, Y., Lu, H., Wu, Z., 2011. Preparation and characterization of a lovastatin-loaded protein-free nanostructured lipid carrier resembling high-density lipoprotein and evaluation of its targeting to foam cells. AAPS PharmSciTech 12, 1200–1208. https://doi.org/10.1208/s12249-011-9668-0.

Haider, M., Abdin, S.M., Kamal, L., Orive, G., 2020. Nanostructured lipid carriers for delivery of chemotherapeutics: A review. Pharmaceutics. https://doi.org/10.3390/pharmaceutics12030288.

Halder, J., Gupta, S., Kumari, R., Gupta, G. Das, Rai, V.K., 2020. Microneedle array: applications, recent advances, and clinical pertinence in transdermal drug delivery. J. Pharm. Innov. https://doi.org/10.1007/s12247-020-09460-2.

Han, F., Li, S., Yin, R., Liu, H., Xu, L., 2008. Effect of surfactants on the formation and characterization of a new type of colloidal drug delivery system: Nanostructured lipid carriers. Colloids Surf. A Physicochem. Eng. Asp. 315, 210–216. https://doi.org/10.1016/j.colsurfa.2007.08.005.

Hao, J., Fang, X., Zhou, Y., Wang, J., Guo, F., Li, F., Peng, X., 2011. Development and optimization of solid lipid nanoparticle formulation for ophthalmic delivery of chloramphenicol using a Box-Behnken design. Int. J. Nanomedicine 6, 683–692. https://doi.org/10.2147/ijn.s17386.

Hao, J., Tong, T., Jin, K., Zhuang, Q., Han, T., Bi, Y., Wang, J., Wang, X., 2017. Folic acid-functionalized drug delivery platform of resveratrol based on Pluronic 127/D-α-tocopheryl polyethylene glycol 1000 succinate mixed micelles. Int. J. Nanomedicine 12, 2279–2292. https://doi.org/10.2147/IJN.S130094.

Hidayah, R., Soeratri, W., Rosita, N., 2018. Development Nanostructured Lipid Carriers (Nlc) Loaded Resveratrol with Different Combination of Soybean Oil and Oleic Acid. Int. J. Adv. Sci. Res. Eng. 4, 64–70. https://doi.org/10.31695/ijasre.2018.32935.

International Conference on Harmonisation of Technical Requirements for Registration of Pharmaceuticals for Human use ICH Harmonised Tripartite Guideline Stability Testing of New Drug Substances and Products Q1A(R2), 2003.

Jain, V., Kumar, H., Anod, H.V., Chand, P., Gupta, N.V., Dey, S., Kesharwani, S.S., 2020. A review of nanotechnology-based approaches for breast cancer and triple-negative breast cancer. J. Control. Release. https://doi.org/10.1016/j.jconrel.2020.07.003.

Jazuli, I., Annu, Nabi, B., moolakkadath, T., Alam, T., Baboota, S., Ali, J., 2019. Optimization of Nanostructured Lipid Carriers of Lurasidone Hydrochloride Using Box-Behnken Design for Brain Targeting: In Vitro and In Vivo Studies. J. Pharm. Sci. 108, 3082–3090. https://doi.org/10.1016/j.xphs.2019.05.001.

Jose, S., Anju, S.S., Cinu, T.A., Aleykutty, N.A., Thomas, S., Souto, E.B., 2014. In vivo pharmacokinetics and biodistribution of resveratrol-loaded solid lipid nanoparticles for brain delivery. Int. J. Pharm. 474, 6–13. https://doi.org/10.1016/j.ijpharm.2014.08.003.

Kaur, P., Garg, T., Rath, G., Goyal, A.K., Murthy, R.R.S., 2016. Development, optimization and evaluation of surfactant-based pulmonary nanolipid carrier system of paclitaxel for the management of drug resistance lung cancer using Box-Behnken design. Drug Deliv. 23, 1912–1925. https://doi.org/10.3109/10717544.2014.993486.

Kayani, Z., Bordbar, A.K., Firuzi, O., 2018. Novel folic acid-conjugated doxorubicin loaded β-lactoglobulin nanoparticles induce apoptosis in breast cancer cells. Biomed. Pharmacother. 107, 945–956. https://doi.org/10.1016/j.biopha.2018.08.047.

Khalil, El-Bary, A.A., Kassem, M.A., Ghorab, M.M., Basha, M., 2013. Influence of formulation parameters on the physicochemical properties of meloxicam-loaded solid lipid nanoparticles. Egypt. Pharm. J. 12, 63. https://doi.org/10.7123/01.EPJ.0000428643.74323.D9.

Khosa, A., Reddi, S., Saha, R.N., 2018. Nanostructured lipid carriers for site-specific drug delivery. Biomed. Pharmacother. https://doi.org/10.1016/j.biopha.2018.04.055.

Ko, J.H., Sethi, G., Um, J.Y., Shanmugam, M.K., Arfuso, F., Kumar, A.P., Bishayee, A., Ahn, K.S., 2017. The role of resveratrol in cancer therapy. Int. J. Mol. Sci. https://doi.org/10.3390/ijms18122589.

Koh, L.L.A., Chandrapala, J., Zisu, B., Martin, G.J.O., Kentish, S.E., Ashokkumar, M., 2014. A comparison of the effectiveness of sonication, high shear mixing and homogenisation on improving the heat stability of whey protein solutions. Food Bioprocess Technol. 7, 556–566. https://doi.org/10.1007/s11947-013-1072-1.

Kosović, E., Topiař, M., Curínová, P., Sajfrtová, M., 2020. Stability testing of resveratrol and viniferin obtained from Vitis vinifera L. by various extraction methods considering the industrial viewpoint. Sci. Rep. 10, 1–9. https://doi.org/10.1038/s41598-020-62603-w.

Kotecha, R., Takami, A., Espinoza, J.L., 2016. Dietary phytochemicals and cancer chemoprevention: A review of the clinical evidence. Oncotarget. https://doi.org/10.18632/oncotarget.9593.

Kumar, A., Sawant, K., 2013. Encapsulation of exemestane in polycaprolactone nanoparticles: Optimization, characterization, and release kinetics. Cancer Nanotechnol. 4, 57–71. https://doi.org/10.1007/s12645-013-0037-4.

Lubrizol, 2010. Viscosity of Carbopol ® * Polymers in Aqueous Systems-Technical data sheet.

Managuli, R.S., Wang, J.T., Faruqu, F.N., Kushwah, V., Raut, S.Y., Shreya, A.B., Al-Jamal, K.T., Jain, S., Mutalik, S., 2019. Asenapine maleate-loaded nanostructured lipid carriers: Optimization and in vitro, ex vivo and in vivo evaluations. Nanomedicine 14, 889–910. https://doi.org/10.2217/nnm-2018-0289.

Manikkath, J., Parekh, H.S., Mutalik, S., 2020. Surface-engineered nanoliposomes with lipidated and non-lipidated peptide-dendrimeric scaffold for efficient transdermal delivery of a therapeutic agent: Development, characterization, toxicological and preclinical performance analyses. Eur. J. Pharm. Biopharm. 156, 97–113. https://doi.org/10.1016/j.ejpb.2020.09.001.

Measuring cell fluorescence using ImageJ — The Open Lab Book v1.0 [WWW Document], n.d. URL https://theolb.readthedocs.io/en/latest/imaging/measuring-cell-fluorescence-using-imagej.html (accessed 1.27.21).

Miura, K., 2020. Measurements of Intensity Dynamics at the Periphery of the Nucleus. pp. 9–32. https://doi.org/10.1007/978-3-030-22386-1_2.

Nagaich, U., Gulati, N., 2016. Nanostructured lipid carriers (NLC) based controlled release topical gel of clobetasol propionate: design and in vivo characterization. Drug Deliv. Transl. Res. 6, 289–298. https://doi.org/10.1007/s13346-016-0291-1.

Nawaz, W., Zhou, Z., Deng, S., Ma, Xiaodong, Ma, Xiaochi, Li, C., Shu, X., 2017. Therapeutic versatility of resveratrol derivatives. Nutrients. https://doi.org/10.3390/nu9111188.

Nayak, A.S., Chodisetti, S., Gadag, S., Nayak, U.Y., Govindan, S., Raval, K., 2020. Tailoring solulan C24 based niosomes for transdermal delivery of donepezil: In vitro characterization, evaluation of pH sensitivity, and microneedle-assisted Ex vivo

permeation studies. J. Drug Deliv. Sci. Technol. 60, 101945 https://doi.org/10.1016/j.jddst.2020.101945.
Nordin, N., Yeap, S.K., Rahman, H.S., Zamberi, N.R., Abu, N., Mohamad, N.E., How, C. W., Masarudin, M.J., Abdullah, R., Alitheen, N.B., 2019. In vitro cytotoxicity and anticancer effects of citral nanostructured lipid carrier on MDA MBA-231 human breast cancer cells. Sci. Rep. 9 https://doi.org/10.1038/s41598-018-38214-x.
Overview for Surface Plot - Minitab [WWW Document], n.d. URL https://support.minitab.com/en-us/minitab/18/help-and-how-to/modeling-statistics/using-fitted-models/how-to/surface-plot/before-you-start/overview/ (accessed 12.8.20).
Patel, S.G., Patel, M.D., Patel, A.J., Chougule, M.B., Choudhury, H., 2018. Solid lipid nanoparticles for targeted brain drug delivery, in: Nanotechnology-Based Targeted Drug Delivery Systems for Brain Tumors. Elsevier, pp. 191–244. https://doi.org/10.1016/B978-0-12-812218-1.00008-7.
Poonia, N., Kaur Narang, J., Lather, V., Beg, S., Sharma, T., Singh, B., Pandita, D., 2019. Resveratrol loaded functionalized nanostructured lipid carriers for breast cancer targeting: Systematic development, characterization and pharmacokinetic evaluation. Colloids Surf. B Biointerfaces 181, 756–766. https://doi.org/10.1016/j.colsurfb.2019.06.004.
Raghu Nandan Reddy, A.S., 2012. SOLID LIPID NANOPARTICLES: AN ADVANCED DRUG DELIVERY SYSTEM | INTERNATIONAL JOURNAL OF PHARMACEUTICAL SCIENCES AND RESEARCH [WWW Document]. Int. J. Pharm. Sci. Res. https://doi.org/https://doi.org/10.13040/IJPSR.0975-8232.4(1).161-71.
Ramöller, I.K., Tekko, I.A., McCarthy, H.O., Donnelly, R.F., 2019. Rapidly dissolving bilayer microneedle arrays – A minimally invasive transdermal drug delivery system for vitamin B12. Int. J. Pharm. 566, 299–306. https://doi.org/10.1016/j.ijpharm.2019.05.066.
Robinson, K., Mock, C., Liang, D., 2015. Pre-formulation studies of resveratrol. Drug Dev. Ind. Pharm. 41, 1464–1469. https://doi.org/10.3109/03639045.2014.958753.
Rute Neves, A., Lúcio, M., Martins, S., Luís Costa Lima, J., Reis, S., Reis REQUIMTE, S., 2013. Novel resveratrol nanodelivery systems based on lipid nanoparticles to enhance its oral bioavailability. Int. J. Nanomedicine 8, 177–187. https://doi.org/10.2147/IJN.S37840.
Shapiro, C.L., Recht, A., 2001. Side effects of adjuvant treatment of breast cancer. N. Engl. J. Med. 344, 1997–2008. https://doi.org/10.1056/NEJM200106283442607.
Silva, C.G., Monteiro, J., Marques, R.R.N., Silva, A.M.T., Martínez, C., Canle L., M., Faria, J.L., 2013. Photochemical and photocatalytic degradation of trans-resveratrol, in: Photochemical and Photobiological Sciences. Royal Society of Chemistry, pp. 638–644. https://doi.org/10.1039/c2pp25239b.
Singh, G., Pai, R.S., 2014. A rapid reversed-phase HPLC method for analysis of trans -resveratrol in PLGA nanoparticulate formulation. ISRN Chromatogr. 2014, 1–6. https://doi.org/10.1155/2014/248635.
Sinha, D., Sarkar, N., Biswas, J., Bishayee, A., 2016a. Resveratrol for breast cancer prevention and therapy: Preclinical evidence and molecular mechanisms. Semin. Cancer Biol. 40–41, 209–232. https://doi.org/10.1016/j.semcancer.2015.11.001.
Sinha, D., Sarkar, N., Biswas, J., Bishayee, A., 2016b. Resveratrol for breast cancer prevention and therapy: Preclinical evidence and molecular mechanisms. Semin. Cancer Biol. https://doi.org/10.1016/j.semcancer.2015.11.001.
Study Forecasts New Breast Cancer Cases by 2030 - National Cancer Institute [WWW Document], n.d. URL https://www.cancer.gov/news-events/cancer-currents-blog/2015/breast-forecast (accessed 10.6.20).
Subramaniam, B., Siddik, Z.H., Nagoor, N.H., 2020. Optimization of nanostructured lipid carriers: understanding the types, designs, and parameters in the process of formulations. J. Nanoparticle Res. https://doi.org/10.1007/s11051-020-04848-0.
Tahara, H., Matsuda, S., Yamamoto, Y., Yoshizawa, H., Fujita, M., Katsuoka, Y., Kasahara, T., 2017. High-content image analysis (HCIA) assay has the highest correlation with direct counting cell suspension compared to the ATP, WST-8 and Alamar blue assays for measurement of cytotoxicity. J. Pharmacol. Toxicol. Methods 88, 92–99. https://doi.org/10.1016/j.vascn.2017.08.003.
Thatipamula, R.P., Palem, C.R., Gannu, R., Mudragada, S., Yamsani, M.R., 2011. Formulation and in vitro characterization of domperidone loaded solid lipid nanoparticles and nanostructured lipid carriers. DARU. J. Pharm. Sci. 19, 23–32.
Tosato, M.G., Maya Girón, J.V., Martin, A.A., Krishna Tippavajhala, V., Lorenzo, Fernández, de Mele, M., Dicelio, L., 2018. Comparative study of transdermal drug delivery systems of resveratrol: High efficiency of deformable liposomes. Mater. Sci. Eng. C 90, 356–364. https://doi.org/10.1016/j.msec.2018.04.073.
Uzunoglu, S., Karaca, B., Atmaca, H., Kisim, A., Sezgin, C., Karabulut, B., Uslu, R., 2010. Comparison of XTT and Alamar blue assays in the assessment of the viability of various human cancer cell lines by AT-101 (-/- gossypol). Toxicol. Mech. Methods 20, 482–486. https://doi.org/10.3109/15376516.2010.508080.
Vatanara, A., Rouholamini Najafabadi, A., Gilani, K., Asgharian, R., Darabi, M., Rafiee-Tehrani, M., 2007. A Plackett-Burman design for screening of the operation variables in the formation of salbutamol sulphate particles by supercritical antisolvent. J. Supercrit. Fluids 40, 111–116. https://doi.org/10.1016/j.supflu.2006.03.028.
Viegas, J.S.R., Praça, F.G., Caron, A.L., Suzuki, I., Silvestrini, A.V.P., Medina, W.S.G., Del Ciampo, J.O., Kravicz, M., Bentley, M.V.L.B., 2020. Nanostructured lipid carrier co-delivering tacrolimus and TNF-α siRNA as an innovate approach to psoriasis. Drug Deliv. Transl. Res. 10, 646–660. https://doi.org/10.1007/s13346-020-00723-6.
Vijayakumar, M.R., Kumari, L., Patel, K.K., Vuddanda, P.R., Vajanthri, K.Y., Mahto, S.K., Singh, S., 2016. Intravenous administration of: Trans -resveratrol-loaded TPGS-coated solid lipid nanoparticles for prolonged systemic circulation, passive brain targeting and improved in vitro cytotoxicity against C6 glioma cell lines. RSC Adv. 6, 50336–50348. https://doi.org/10.1039/c6ra10777j.
Xiao, Q., Zhu, W., Feng, W., Lee, S.S., Leung, A.W., Shen, J., Gao, L., Xu, C., 2019. A review of resveratrol as a potent chemoprotective and synergistic agent in cancer chemotherapy. Front. Pharmacol. https://doi.org/10.3389/fphar.2018.01534.
Younas, M., Hano, C., Giglioli-Guivarc'H, N., Abbasi, B.H., 2018. Mechanistic evaluation of phytochemicals in breast cancer remedy: Current understanding and future perspectives. RSC Adv. 8, 29714–29744. https://doi.org/10.1039/c8ra04879g.
Yuan, H., Chen, J., Du, Y.Z., Hu, F.Q., Zeng, S., Zhao, H.L., 2007. Studies on oral absorption of stearic acid SLN by a novel fluorometric method. Colloids Surf. B Biointerfaces 58, 157–164. https://doi.org/10.1016/j.colsurfb.2007.03.002.
Yuan, H., Miao, J., Du, Y.Z., You, J., Hu, F.Q., Zeng, S., 2008. Cellular uptake of solid lipid nanoparticles and cytotoxicity of encapsulated paclitaxel in A549 cancer cells. Int. J. Pharm. 348, 137–145. https://doi.org/10.1016/j.ijpharm.2007.07.012.
Zhang, W., Li, X., Ye, T., Chen, F., Yu, S., Chen, J., Yang, X., Yang, N., Zhang, J., Liu, J., Pan, W., Kong, J., 2014. Nanostructured lipid carrier surface modified with Eudragit RS 100 and its potential ophthalmic functions. Int. J. Nanomedicine 9, 4305–4315. https://doi.org/10.2147/IJN.S63414.
Zirak, M.B., Pezeshki, A., 2015. Effect of Surfactant Concentration on the Particle Size, Stability and Potential Zeta of Beta carotene Nano Lipid Carrier, Int. J. Curr. Microbiol. App. Sci.
Zu, Y., Zhang, Y., Wang, W., Zhao, X., Han, X., Wang, K., Ge, Y., 2014. Drug Delivery Preparation and in vitro/in vivo evaluation of resveratrol-loaded carboxymethyl chitosan nanoparticles. https://doi.org/10.3109/10717544.2014.924167.
Zur Mühlen, A., Schwarz, C., Mehnert, W., 1998. Solid lipid nanoparticles (SLN) for controlled drug delivery - Drug release and release mechanism. Eur. J. Pharm. Biopharm. 45, 149–155. https://doi.org/10.1016/S0939-6411(97)00150-1.